Synaptic mechanisms modulate the spatiotemporal dynamics of striatal direct pathway neurons and motor output

John J Marshall[1,*], Jian Xu[1], Nai-Hsing Yeh[1], Seongsik Yun[1], Toshihiro Nomura[1], John N Armstrong[1], Jones G Parker[1,2,3,*], Anis Contractor[1, 2, 4,*]

[1]Department of Neuroscience, Feinberg School of Medicine, Northwestern University, Chicago IL 60611.

[2]Department of Psychiatry and Behavioral Sciences, Feinberg School of Medicine, Northwestern University, Chicago IL 60611.

[3]Department of Pharmacology, Feinberg School of Medicine, Northwestern University Chicago IL 60611.

[4]Department of Neurobiology, Weinberg School of Arts and Sciences, Northwestern University, Evanston IL 60201.

Correspondence: *John J Marshall
Dept of Neuroscience
Northwestern University Feinberg School of Medicine
303 E. Chicago Ave
Chicago, Il 60611
j-marshall@northwestern.edu
Tel: 312 503 0276

*Jones G Parker
Dept of Neuroscience
Northwestern University Feinberg School of Medicine
303 E. Chicago Ave
Chicago, Il 60611
Jones.parker@northwestern.edu
Tel: 312 503 3165

*Anis Contractor
Dept of Neuroscience
Northwestern University Feinberg School of Medicine
303 E. Chicago Ave
Chicago, Il 60611
Jones.parker@northwestern.edu
Tel: 312 503 3165

Words in Abstract – 206
Introduction – 908
Discussion - 1887
Number of Pages - 47
Number of Figures - 5

Abstract

Striatal spiny-projection neurons (SPNs) integrate glutamatergic inputs from the motor cortex and thalamus with neuromodulatory signals to regulate motor output. *In vivo* Ca^{2+} imaging has demonstrated that spatially overlapping ensembles of direct and indirect pathway SPNs (dSPNs, iSPNs) are co-active during spontaneous movement. This co-activity is statistically greater among nearby neurons, correlates with behavioral state, and changes in an SPN-type-specific manner under pathological conditions. How this co-activity arises and whether is important for movement are not well understood. Co-activity likely arises from shared excitatory inputs, the strength of which are scaled by well-characterized mechanisms of synaptic plasticity. Here, we show that the Group I metabotropic glutamate receptor 5 (mGluR5), which regulates the strength of corticostriatal synapses, is a key mediator of behaviorally relevant SPN co-activity. Pharmacological modulation of mGluR5 signaling bidirectionally altered movement and co-activity, but not the absolute level of activity in dSPNs. Targeted deletion of mGluR5 in dSPNs recapitulated the effects on spatiotemporal neural dynamics and movement, consistent with a striatum-specific effect of mGluR5 modulation. Targeted deletion of mGluR5 also produced changes in the synaptic properties of dSPNs. Separate from any effects on overall activity, our results show that excitatory synaptic modulation influences motor function by coordinating the spatial co-activation of dSPNs *in vivo*.

Introduction

The dorsal striatum is central to movement initiation and to regulating the kinematics of learned movements [1,2]. Synaptic plasticity in this input structure of the basal ganglia has been demonstrated to be important for motor learning [3]. In particular, the strength of corticostriatal synapses between the motor cortex and spiny-projection neurons (SPNs) in the dorsolateral striatum (DLS) are strengthened by learning a motor sequence [4] or during the acquisition of a motor skill [5,6]. These glutamatergic, corticostriatal inputs form synapses onto two types of SPNs that are distinguished by their expression of dopamine receptor subtypes and downstream axonal projections. The D1 dopamine

receptor-expressing, or direct pathway SPNs (dSPNs) project monosynaptically to the output nuclei of the basal ganglia, the substantia nigra pars reticulata (SNr) and globus pallidus internal segment (GPi). By contrast, D2 dopamine receptor-expressing SPNs (iSPNs) project indirectly to basal ganglia output nuclei via the globus pallidus external segment (GPe) and the subthalamic nucleus (STN) [7]. In classical models of the basal ganglia circuit, activity in dSPNs facilitates movement and activity in iSPNs inhibits movement. Therefore, the relative level of activity between the two populations is predicted to correlate with an animal's motor state (*e.g.*, moving or at rest).

This rate-model framework of striatal function garnered early support from anatomical and pharmacological observations as well as findings from studies investigating the neuropathology of striatum-related neurodegenerative disease [8]. However, the model is inconsistent with more recent observations employing *in vivo* imaging techniques. In these studies, where the activity of genetically defined iSPNs and dSPNs can be monitored concurrently in awake behaving animals, dSPNs and iSPNs are consistently co-active during movement initiation and procession through movement sequences [9]. More recently, it was shown that dSPNs and iSPNs simultaneously activate with spatially clustered dynamics, and that this spatiotemporal organization is important for motor control [10-12]. Spatiotemporal clustering, or heightened co-activity among proximal SPN pairs, is most pronounced during periods of rest, but also transiently increases during transitions from rest to movement then subsides as SPNs become more active during movement progression [10-13]. Importantly, dopamine signaling appears to play an important role in sculpting these dynamics. The loss of dopamine diminishes the spatiotemporal coordination of iSPN activity, while heightened dopamine release de-correlates activity in dSPNs and heightens iSPN co-activity [10-13].

Although the mechanisms that constrain the spatiotemporal coordination of dSPN and iSPN activity are not precisely known, SPNs have hyperpolarized resting membrane potentials that prevent action potential generation in the absence of glutamatergic input [14,15]. Given that glutamate is required for SPN activation, and given dopamine's role in modifying the strength of glutamatergic synapses in SPNs, it is likely

102 that synaptic plasticity influences the spatiotemporal dynamics of SPNs by regulating
103 their collective sensitivity to convergent excitatory inputs [16,17].

104 dSPNs and iSPNs receive excitatory input from the cortex and thalamus. Cortico-
105 and thalamostriatal synapses differ in their expression of pre- and post-synaptic
106 neurotransmitter receptors and forms of synaptic plasticity[18]. Extensive *in vitro* work has
107 demonstrated various mechanistically distinct types of long-term potentiation (LTP) and
108 long-term depression (LTD) at cortical inputs to dSPNs and iSPNs [19,20]. While the range
109 of physiological and neuromodulatory mechanisms of corticostriatal plasticity are
110 complex, one well-studied type of plasticity is endocannabinoid (eCB) dependent LTD,
111 induced *in vitro* by moderate to high frequency stimulation of corticostriatal inputs paired
112 with postsynaptic depolarization [18]. Importantly, corticostriatal LTD requires activation of
113 postsynaptic Gq-linked, Group I metabotropic glutamate receptors (mGluRs). mGluR
114 activation causes the mobilization of endocannabinoids (eCBs) from the postsynaptic
115 neuron which act as a retrograde signal by activating presynaptic CB1 receptors to
116 reduce the release probability of glutamatergic corticostriatal synapses [21]. mGluR LTD
117 occurs at corticostriatal synapses in both dSPNs and iSPNs [22] but not at thalamostriatal
118 synapses [18]. eCB release and retrograde signaling can also produce transient
119 modulation of presynaptic release to cause the short-term depression of corticostriatal
120 synapses [23,24], similar to what has been observed at synapses in several other brain
121 regions [25]. Despite extensive *in vitro* work, little is known about the circumstances under
122 which eCB-dependent synaptic modulation occurs *in vivo* and how it may relate to
123 motor behavior. Moreover, it is unknown how the modulation of corticostriatal synaptic
124 strength regulates the level and/or spatiotemporal dynamics of SPN activity with respect
125 to movement.

126 In the striatum, mGluR5 has been shown to have a prominent role in mGluR-
127 dependent synaptic plasticity. Therefore, we asked whether mGluR5 signaling
128 contributes to voluntary movement and the dynamics of dSPN activity in the DLS. We
129 found that manipulating mGluR5 signaling had bidirectional effects on movement and
130 the spatiotemporal dynamics of dSPN activity, with minimal effects on their overall
131 levels of activity. Specifically, using *in vivo* Ca^{2+} imaging we found that pharmacological

132 inhibition of mGluR5 signaling produced a reduction in spontaneous movement and
133 heightened the spatially clustered patterns of co-activity in dSPNs, whereas positive
134 modulation of mGluR5 signaling had the opposite effects. Consistent with these
135 findings, conditional knockout of mGluR5 in dSPNs (D1 cKO mice) had minimal effects
136 on the levels of dSPN or iSPN activity but specifically increased the spatiotemporal
137 coordination of dSPN activity and reduced spontaneous locomotion. Collectively, these
138 findings suggest that mGluR-mediates synaptic plasticity mechanisms bidirectionally
139 constrain the spatiotemporal coordination, but not the levels of dSPN activity, into states
140 that correlate with increased or decreased locomotor activity. Our study lays the
141 groundwork for dissociating the separable roles of the activity rates versus patterning of
142 SPN activity in motor control and has implications for correcting disruptions of this
143 patterning in basal ganglia-associated diseases.

144 **Results**

145 *dSPNs exhibit spatially clustered activity that varies with movement*

146 There is a strong correlation between spatiotemporal patterns of SPN activity and motor
147 output [10-12], but it is not known if synaptic properties modulate this coordinated activity *in*
148 *vivo*. To assess the activity of dSPNs during spontaneous motor behavior, we implanted
149 gradient refractive index (GRIN) lenses into the dorsolateral striatum of mice expressing
150 Cre-recombinase in dSPNs under the control of the *Drd1a* promoter. A Cre-dependent
151 AAV to express GCaMP6f was introduced either by a prior stereotaxic injection of virus
152 or by coating the lenses with a silk fibroin film containing the AAV (**Figure 1a**) [26]. The
153 GRIN lens was coupled to a head-mounted miniscope for 1P imaging of somatic Ca^{2+}
154 events[27]. **Figure 1b** shows an example of a field of view from one mouse and the
155 segmented outlines of neurons after processing of the videos (*see* **Methods**) and
156 examples of individual dSPN Ca^{2+} dynamics (**Figure 1c**). Consistent with prior
157 observations [13], Ca^{2+} event rates in dSPNs increased during periods of movement
158 (**Figure 1d, e**). The probability of a Ca^{2+} events in detected cells (defined as
159 fluorescence change of 2.5× the baseline for each cell, *see* **Methods**) increased during
160 movement (**Figure 1d**) and the Ca^{2+} event rate increased with increasing animal
161 velocity (**Figure 1e**). Previous work has demonstrated that dSPNs and iSPNs are

162 spontaneously co-active in spatially intermingled clusters, a feature that has been
163 proposed to be important for action selection [10-12,28]. To examine this spatiotemporal
164 coordination and its modulation by movement state, we measured dSPN co-activity
165 using a Jaccard index of dSPN pairs as a function of the Euclidean distance between
166 the cell pairs in the DLS. This measure captures co-activity between neuron pairs (as
167 opposed to co-inactivity) more specifically than a linear correlation coefficient (**Figure**
168 **1f; Methods**) [11]. Across all cell pairs in the field-of-view for each session, a correlation
169 matrix was generated in which, for each frame of the recording, the cell pair was scored
170 a 1 if both cells were active, or 0 otherwise. These scores for each frame were divided
171 by the number of events in both cells to generate a co-activity score for that pair. **Figure**
172 **1f** shows schematized raster plots to demonstrate this process. Then, those values
173 were normalized to averages measured from independently shuffled Ca^{2+} traces for
174 each cell in the recording (using 1000 independent shuffles for each cell trace), to
175 control for changes in mean activity level between conditions (**Figure 1f**). If cells were
176 co-active independently of distance, then a plot of co-activity normalized to the shuffled
177 data as a function of distance would be flat (**Figure 1g, top**), while clustered co-activity
178 (*i.e.*, higher among proximal cells) would show a downward sloping curve (**Figure 1g,**
179 **bottom**). Consistent with prior reports [10-12], this analysis revealed that co-activity among
180 neuron pairs is markedly higher among proximal cells and decreases with increasing
181 Euclidean distance between pairs (**Figure 1h, top**). Furthermore, as we had previously
182 demonstrated, co-activity among all pairs was higher during rest and decreased during
183 periods of movement (**Figure 1h, top**) [13].

184 We next quantified the extent to which activity was higher in proximal cells versus
185 distal neurons in each frame of the recording using a spatial coordination index (SCI),
186 as defined previously [11]. Here, for each frame of the down-sampled video, we preserved
187 the cell activity traces but shuffled the pairwise distances for each neuron pair. We then
188 performed a pair of Kolmogorov–Smirnov tests (**methods**) to determine if the
189 cumulative distribution of active cell distances in each frame was smaller (*i.e.*, left-
190 shifted or more “clustered”) or greater (right-shifted or less “clustered”) than that of the
191 shuffled data. This analysis allows for visualization of how the spatiotemporal dynamics
192 SPN activity change instantaneously (*e.g.*, during movement onset). Consistent with

193 that reported previously, the degree of “clustered” activity quantified in this way
194 increased significantly during movement onset (within 2.5 seconds of the mouse
195 initiating movement) [11]. This transient increase contrasts with the increased basal co-
196 activity at all cell-cell distances seen during periods when mice were at rest (defined as
197 centroid velocity below a given threshold).

198 *The spatiotemporal dynamics of dSPN activity is modulated by mGluR5*

199 The dominant form of synaptic plasticity at corticostriatal synapses is mediated by
200 Group1 mGluRs [18], and the primary receptor of this class expressed in SPNs is mGluR5
201 [29]. Germline deletion of mGluR5 causes significant motor phenotypes, but it is not
202 known how mGluR5 signaling directly affects motor function [30]. Due to the known
203 importance of mGluR5 in modulating synaptic weight at corticostriatal synapses, we
204 hypothesized that pharmacological modulation of mGluR5 would affect SPN dynamics
205 *in vivo*.

206 To assess the effects of modulating mGluR5 activity on dSPN dynamics during
207 spontaneous behavior, we injected mice with vehicle or the mGluR5 negative allosteric
208 modulator (NAM) fenobam (26 mg/kg via i.p. injection) immediately prior to a 60-minute
209 open field test. We analyzed dSPN activity from 8 animals expressing GCaMP6f in
210 dSPNs and implanted with GRIN lenses in the DLS (**Figure 2a–c**). We measured
211 activity as mice spontaneously explored the open field arena. On average we recorded
212 from 91 dSPNs per mouse in these experiments.

213 Fenobam treatment uniformly reduced locomotion (**Figure 2d, e**), an effect that
214 was driven more by a reduction in movement bout duration than the frequency of
215 movement bouts (**Figure 2f**). Interestingly, dSPN event rates were unchanged following
216 fenobam injection, with Ca^{2+} event rates in dSPNs increasing with spontaneous
217 locomotor speed across the range of running speeds in both fenobam and vehicle
218 injected animals (**Figure 2g**). Fenobam also had no effect on the amplitude or duration
219 of Ca^{2+} events (**Figure 2 supplement**).

220 However, fenobam treatment significantly increased the pairwise co-activity of
221 dSPNs across the whole range of cell-cell distances (**Figure 2h**). Notably, while co-

222 activity at all distances was enhanced by fenobam treatment, we did not resolve any
223 differences in spatial coordination, measured using the SCI, between vehicle and drug
224 treatment as animal transitioned from rest to movement. In both cases, the SCI peaked
225 around the time of movement onset (**Figure 2i**). This suggests that the most significnat
226 effect of mGluR5 on dSPN co-activity is to increase its overall extent, rather than the
227 relative extent to which it becomes more or less "clustered" during behavioral state
228 transitions. As fenobam treatment reduced movement, and co-activity is modulated by
229 movement, we separated our analysis into periods of movement and rest to compare
230 equivalent behavioral states during vehicle and drug treatment. While fenobam
231 treatment increased dSPN co-activity during both rest and movement, its effects were
232 most pronounced during periods of rest (**Figure 2j, k**). However, in analyzing the
233 relative increase in coactivity between rest and movement, there was no significant
234 difference between fenobam and vehicle treated animals (**Figure 2l**).Taken together
235 these results suggest that fenobam may suppress movement by transitioning
236 spatiotemporal dSPN ensemble dynamics towards a rest-associated state of high
237 overall co-activity,without affecting the absolute rates of their activity. In this rest-
238 associated state, overall neuronal activity is reduced but more correlated, resulting in a
239 higher degree of co-activity.

240 *An mGluR5 positive allosteric modulator (PAM) increases movement and decreases*
241 *SPN co-activity*

242 Next, we sought to determine how promoting mGluR5 signaling affects motor output
243 and SPN dynamics. We selected JNJ-46778212/VU0409551 (JNJ) an mGluR5 PAM
244 with demonstrated *in vivo* efficacy and known pharmacokinetics in mice [31]. We
245 administered JNJ (100 mg/kg) or vehicle via i.p. injection 30 minutes prior to measuring
246 dSPN dynamics for one hour during locomotion in an open field arena. In contrast to
247 fenobam, JNJ treatment decreased the amount of time the animal spent at rest (**Figure**
248 **3a**). However, there was no statistically significant effect on mean velocity (**Figure 3b**),
249 number of bouts (Figure 3c), or bout length (**Figure 3d**). Like fenobam, JNJ did not
250 affect the levels of dSPN activity when measured as a function of the animal's running
251 speed (**Figure 3e**). Additionally, there was no effect on the amplitude or duration of Ca^{2+}

events (**Figure 3 supplement**). However, JNJ significantly decreased the co-activity among dSPN cell pairs measured across a range of Euclidean distances (**Figure 3f**). Again, as with fenobam, animals from both the vehicle and drug treatment groups showed significant increases in spatial coordination surrounding movement onset (**Figure 3g**). The effect on overall co-activity was most pronounced, and statistically significant, during periods of rest (**Figure 3i, j**). Therefore, JNJ treatment had effects that were qualitatively inverse to the effects of fenobam on locomotion and dSPN co-activity during periods of rest. These findings are consistent with the idea that JNJ promoted movement by inducing movement-associated dSPN ensemble dynamics by de-correlating their activity.

mGluR5 activation in the striatum results in the mobilization of eCBs, specifically 2-AG, in dSPNs[21,23-25]. Therefore, we asked whether enhancing eCB levels by preventing 2-AG degradation using the monoacylglycerol lipase (MAGL) inhibitor JZL-184 affected the spatiotemporal dynamics of dSPN activity. We administered to mice JZL-184 (10 mg/kg i.p.) before recording dSPN Ca^{2+} activity for 60 minutes in an open field arena. Interestingly, in contrast to the mGluR5 PAM, JZL-184 significantly reduced rate of Ca^{2+} events (**Figure 3k**) but did not affect the co-activity of dSPNs (**Figure 3l**). These results suggest that broadly enhancing eCB levels does not recapitulate the effects of potentiating mGluR5 signaling specifically.

Collectively these results demonstrate that potentiating mGluR5 signaling shifts dSPN dynamics to a less correlated state, while inhibiting mGluR5 signaling enhances the correlated state of dSPNs. It is notable that spontaneous dSPN activity is less correlated during periods of movement than rest, and de-correlated dSPN activity has been shown to occur in hyperkinetic states (*e.g.*, dyskinetic and hyperdopaminergic states [11,13]). These observations suggest that inhibition of mGluR5 signaling suppresses movement by altering the spatiotemporal dynamics of dSPNs through synaptic mechanisms that alter their collective recruitment via excitatory afferents.

mGluR5 reduces corticostriatal glutamatergic transmission at dSPN synapses in the dorsolateral striatum

281 Our experiments demonstrated changes in striatal dSPN network activity that correlate
282 with changes in motor behavior mediated by pharmacologically modulating mGluR5. To
283 determine whether modulating mGluR5, specifically in striatal dSPNs, mediates the
284 observed effects on locomotor and striatal activity, we used a genetic approach to
285 selectively manipulate mGluR5 in D1 receptor-expressing neurons. To do this, we
286 crossed *Grm5*$^{fl/fl}$ mice [32] to D1-Cre mice [33] to create conditional knockout mice (D1 cKO)
287 mice. Further crossing with a Cre reporter allele (Ai9) [34] enabled us to perform patch-
288 clamp recordings from visually identified dSPNs in striatal slices to record corticostriatal
289 EPSCs (**Figure 4a**). As we have previously demonstrated [24], a ten-minute application of
290 the group 1 mGluR agonist DHPG (100 μM) caused a depression of EPSCs in WT
291 recordings (**Figure 4b**). This effect was significantly diminished in recordings from cKO
292 mice, demonstrating a disruption of mGluR5 signaling (**Figure 4c**).

293 A number of behavioral phenotypes have been described in mice with
294 constitutive, germline *Grm5* deletion [30]. Given our previous observations and the fact
295 that SPN activity in the dorsal striatum is important for motor control, we asked whether
296 selective ablation of *Grm5* in dSPNs affected locomotion and motor learning. Tracking
297 distance traveled in the open field, we found that the D1 cKO mice had reduced
298 spontaneous locomotion (**Figure 4d**) and displayed a reduction in total distance
299 traveled (**Figure 4e**). We also found the D1 cKO mice had diminished digging behavior
300 in a novel environment (**Figure 4f**). Taken together these results demonstrate that
301 selectively disrupting mGluR5 signaling in dSPNs reduces spontaneous movement in
302 novel environments.

303 To measure locomotion in the home cage setting, we introduced running wheels
304 and monitored activity over 7 days. During the first 3 days, D1 cKO mice demonstrated
305 significantly reduced voluntary running (**Figure 4h, i**). However, both control and D1
306 cKO mice increased the time spent running over the course of 7 days such that the
307 difference between the groups was not significant by day 7 (**Figure 4i**).

308 Finally, on an accelerating rotarod D1 cKO mice showed a consistently reduced
309 latency to fall over the course of 12 training trials across three days (**Figure 4g**).
310 Despite this deficit, D1 cKO mice did improve over the course of training, indicating that

311 they were capable of learning the task. Thus, the D1 cKO mice exhibited a primary
312 deficit in spontaneous motor activity with only minor deficits in the learned motor tasks
313 of running on a wheel or forced locomotion on the rotarod.

314 Because of the clear motor phenotype in D1 cKO mice, we determined whether
315 there were any changes in the intrinsic or synaptic properties of dSPNs in these mice.
316 Whole-cell current-clamp recordings from visually identified dSPNs expressing
317 tdTomato found no difference in the voltage response to increasing current injection
318 suggesting no alteration in the intrinsic excitability of dSPNs in D1 cKO mice (**Figure 4j,**
319 **k**). In recordings of mEPSCs, that reflect all excitatory synapses (corticostriatal and
320 thalamostriatal), we found that the amplitudes of mEPSCs were unchanged, but their
321 frequency was significantly increased in dSPNs from D1 cKO mice (**Figure 4l–m**),
322 indicating increased release probability when mGluR5 expression is disrupted.

323 *Spatiotemporal activity of dSPNs is disrupted in D1 cKO mice*

324 To measure the *in vivo* dynamics of dSPNs in D1 cKO mice, we implanted GRIN lenses
325 into the DLS of control and D1 cKO mice and analyzed dSPN Ca^{2+} activity during 20
326 minutes of open field exploration (**Figure 5a–e**). We performed control imaging
327 experiments in mice expressing Cre in dSPNs but with the wild type *GRM5* allele (D1
328 cre; *GRM5* +/+). Consistent with our previous results, the event rate of dSPN Ca^{2+}
329 transients increased with locomotor speed in both experimental and control mice
330 (**Figure 5d**). Selective mGluR5 deletion in *Drd1a*-expressing neurons did not alter the
331 rate of dSPN Ca^{2+} events compared to control mice (**Figure 5d**). cKO mice and control
332 animals also showed similar distributions of event amplitudes and durations (**Figure 5**
333 **supplement**). Instead, the normalized coactivity of dSPNs (analyzed across 50-μm bins
334 of pairwise cell distances) was significantly increased in D1R cKO mice, similar to the
335 effect of the mGluR5 NAM fenobam (**Figure 5e**). Additionally, D1R cKO mice and
336 control mice showed a transient peak in coactivity surrounding motion onset (**Figure 5f)**.
337 When measured over all frames, the coactivity in both control and cKO mice increased
338 during continuous period of rest compared to periods of continuous movement, however
339 there was no difference in this effect between groups (**Figure 5g)**. Therefore, targeted

340 genetic deletion of mGluR5 in dSPNs had qualitatively similar effects as systemic
341 administration of the mGluR5 NAM on co-activity of dSPNs.

342 Finally, because both dSPNs and iSPNs exhibit spatially clustered activity *in vivo*,
343 and because they are synaptically connected through recurrent collaterals [35], it is
344 possible that disruption of mGluR5 signaling in dSPNs may also affect the levels and
345 spatiotemporal dynamics of activity in intermingled iSPNs. To address this question, we
346 used a viral "Cre-off" strategy to express GCaMP6 in Cre-negative, iSPNs of *Drd1a*-Cre;
347 *Grm5*$^{fl/fl}$ mice[36]. We found that the deletion of mGluR5 in dSPNs had no effects on either
348 the levels of activity in iSPNs (**Figure 5h**) or their spatiotemporal clustering (**Figure 5i**).
349 Therefore, the alteration in SPN dynamics in D1 cKO mice appear to be cell-
350 autonomous, as specific targeting of mGluR5 in dSPNs did not affect iSPN activity in D1
351 cKO mice.

352 Together, these results demonstrate that the manipulation of mGluR5 signaling,
353 through pharmacological or targeted genetic means, leads to changes in the
354 spatiotemporal patterns of activity in dSPNs with minimal effects on their overall levels
355 of activity. Notably, these spatiotemporal dynamics varied with locomotor speed under
356 normal conditions, and manipulations of mGluR5 signaling induced changes in these
357 dynamics that correlated with locomotor state. These findings suggest that these two
358 facets of activity—levels and spatiotemporal patterning of activity—are separable and
359 provide important insights into the role of spatiotemporally coordinated activity in the
360 generation of movement.

361 **Discussion**

362 The rate-model of basal ganglia function posits that activity in dSPNs and iSPNs have
363 distinct and opposing effects on movement. This framework is primarily based on
364 anatomical evidence from the distinct projection targets of dSPNs and iSPNs and
365 electrophysiological recordings in their downstream projection targets under conditions
366 modeling parkinsonism [8]. These target nuclei inhibit motor control nuclei in the hindbrain
367 mesencephalic locomotor region and thalamic regions that project to the motor cortex
368 [37,38]. In this context, dSPN activation is predicted to increase activity in these motor

369 control regions to facilitate movement, while iSPN activation is predicted to decrease
370 activity in these same regions to inhibit movement.

371 However, this classical model is not supported by recent *in vivo* imaging studies
372 using fiber photometry or endoscopy to record Ca^{2+} activity in genetically specified
373 dSPNs or iSPNs. In contrast to the predictions of the rate-model, dSPNs and iSPNs are
374 indistinguishably responsive to increases and decreases in movement [9]. Intriguingly, *in*
375 *vivo* endoscopy has shown that overlapping clusters of dSPNs and iSPNs co-activate
376 during movement, with small but statistical correlations between the activation of
377 different clusters during different movement types [10]. These findings suggest an
378 alternative model where, in contrast to the relative level of activity in each SPN type, the
379 degree of co-activity among SPNs and ensemble identity may be important for
380 specifying proper motor output.

381 Despite evidence that SPNs may influence movement via the coordination of
382 their activity, the biological mechanisms responsible for these coordinated patterns are
383 not known. Seminal *in vitro* electrophysiology studies demonstrated that SPNs fire
384 action potentials coincident with large excitatory inputs that shift their resting membrane
385 potential to transiently stable, depolarized "up" states [14,15]. These excitatory inputs arise
386 from the cortex and thalamus. Our results suggest that the modulation of the synaptic
387 weight, particularly at corticostriatal synapses where several forms of plasticity require
388 mGluR5 receptors, is a crucial mechanism constraining the patterns of dSPN co-activity
389 in states associated with movement or rest.

390 *Spontaneous motor output correlates with the level of coactivity in dSPNs*

391 In the current work, we used pharmacological and genetic manipulations to examine
392 how activity in dSPNs varies with movement while targeting the receptor controlling the
393 dominant form of synaptic plasticity in the DLS. Systemic administration of the mGluR5
394 negative allosteric modulator, fenobam, led to significant increases in co-activity among
395 dSPNs and reduced locomotor activity. By contrast, systemic administration of the
396 mGluR5 positive allosteric modulator JNJ decreased dSPN co-activity and increased
397 locomotion. Notably, neither pharmacological manipulation of mGluR5 led to significant
398 changes in the rate of dSPN Ca^{2+} events. Our results suggest a model whereby either

399 potentiating or inhibiting mGluR5 signaling alters the recruitment of dSPNs such that the
400 overall activity level is preserved but that the patterns of their co-activity change in a
401 manner that corresponds to motor output. This is further confirmed by our data from
402 animals with targeted deletion of mGluR5 in dSPNs, which similarly showed no change
403 in event rate but an increase in co-activity.

404 Our results are consistent with prior analysis demonstrating that the co-activity
405 among pairs of dSPNs is higher at rest than during movement [13]. Here we found that
406 pharmacological manipulations that alter these clustered co-activity states
407 correspondingly alter the levels of spontaneous motor output. Specifically, shifting the
408 dSPN network to a level of higher co-activity, as with fenobam treatment or mGluR5
409 deletion in dSPNs, leads to a reduction in the amount of time animals spent moving. By
410 contrast, potentiating mGluR5 receptors with systemic JNJ administration led to an
411 increase in time spent moving and a corresponding decrease in the dSPN co-activity.

412 Our *ex vivo* electrophysiology data from cKO animals further supports these
413 conclusions, as disrupting endogenous mGluR5 signaling in dSPNs does not result in
414 changes in the excitability of neurons. Instead, genetic deletion of mGluR5 altered the
415 synaptic properties of dSPNs, likely an adaptive response consistent with the
416 established role of mGluR5 in regulating corticostriatal synaptic weights. These findings
417 suggest that these selective changes in synaptic plasticity may underlie the altered
418 spatiotemporal patterning of dSPN activity without changes in their overall levels of
419 activity observed *in vivo*.

420 It is important to note that, in our pharmacological experiments, we observed that
421 inhibition of mGluR5 with systemically administered fenobam increased the co-activity
422 among active neuron pairs across all distance bins we measured. That is, co-activity
423 was increased in both proximal and distal neuron pairs and this increased co-activity
424 correlated with decreased ambulatory behavior. Administration of an mGluR5 PAM
425 decreased co-activity when measured across all binned distances of neuron pairs and
426 this occurred in coincidence with increased ambulatory behavior. It has previously been
427 demonstrated [11], and we replicated here, that surrounding movement onsets there is an
428 increase in the extent to which proximal neuron pairs are statistically more likely to be

429 co-active than distal neuron pairs. Using a previously established metric for quantifying
430 this increase, the spatial correlation index, we did not resolve any significant changes in
431 the onset related changes in this metric following either genetic or pharmacological
432 alterations of mGluR5 activity. Our central finding, observed with both pharmacological
433 and genetic manipulations, is that manipulating mGluR5 signaling alters overall dSPN
434 co-activity, irrespective of cell proximity, in a manner that correlates with changes in
435 motor output. We hypothesize that these changes are likely due to alterations in
436 synaptic weight at dSPN synapses that occur following mGluR5 manipulation.

437 One way in which mGluR5 may modify synaptic weight is through long-term
438 plasticity. *In vitro* studies have demonstrated that mGluR5 activation occurs following
439 pairing of postsynaptic depolarization with moderate to high frequency excitatory
440 synaptic input [21]. mGluR5 activation can result in the long-term depression (LTD) of
441 synaptic transmission or a more transient depression in release probability [23,24,39]. If rest
442 associated ensembles of dSPNs are substantially different in composition from
443 movement and/or movement-onset ensembles, then our data suggests that synapses
444 onto dSPNs may have a lower synaptic weight during spontaneous behavior than
445 movement or movement onset ensembles, potentially due to eCB release. Inhibiting
446 mGluR5, either through pharmacology or genetics, may increase this synaptic weight,
447 thereby promoting activation of rest ensembles and decreasing motor output. This input
448 that primarily governs the activation of movement-related ensembles could either be a
449 separate population of cortical inputs with higher synaptic weight or thalamostriatal
450 inputs more resilient to mGluR5 manipulations [18].

451 Our results are an important step in understanding how the regulation of synaptic
452 weights by mGluR5 may act on the coordinated activity of dSPNs *in vivo* to regulate
453 behavior.

454 *Global enhancement of eCB levels does not alter clustered co-activity*

455 The lack of change in spatiotemporal coordination following systemic administration of
456 the 2-AG degradation inhibitor JZL-184 suggests that global enhancement of eCB levels
457 does not produce a similar outcome as modulating mGluR5 signaling. However, in
458 contrast to selective mGluR5 modulation we did observe a reduction in overall dSPN

459 event rates with JZL. One possibility is that a degree of synaptic specificity is required to
460 affect clustered activation of dSPNs. Thus, JZL treatment may have exerted such broad
461 effects on the circuit that it resulted in a different outcome for neural clustering and
462 motor output than that observed following treatment with the allosteric modulators of
463 mGluR5 receptors that modify the weight of specific active synapses.

464 These results support a model whereby the level of co-activity among specific
465 groups of dSPNs is potentially important for controlling motor output. Therefore, globally
466 altering the synaptic weights of all neurons may overshadow the results of synaptic
467 alterations in specific subsets of SPNs. This idea is consistent with the notion that
468 individual dSPNs may be precisely tuned to have specific roles in regulating motor
469 output, such that altering the activity of one dSPN subgroup would not have the same
470 effect as altering the activity of a different sub-group. This interpretation is also at odds
471 with the classical rate-based models of SPN activity.

472

473 *Role of non-dSPN mGluR5 receptors in regulating movement*

474 There are notable differences in the design of our experiments using conditional
475 deletion of mGluR5 from dSPNs and systemic administration of a negative allosteric
476 modulator of mGluR5. Following fenobam administration, we observed a significant
477 increase in co-activity when animals were at rest and a smaller increase during
478 movement, however the relative increase in coactivity between rest and movement did
479 not differ significantly from controls in either cKO animals or following fenobam
480 treatment. Therefore, in both cases, inhibition of mGluR5 may promote the activation of
481 rest ensembles and thereby inhibit motor output.

482 Within the striatum alone, mGluR5 is expressed in iSPNs and interneurons and
483 modulation of these cell types by systemically administered compounds could produce
484 changes in behavior and striatal circuit function. dSPNs receive GABAergic input from
485 both iSPNs as well as striatal interneurons. Of particular note, parvalbumin-positive fast-
486 spiking interneurons also receive excitatory input from the cortex and provide
487 feedforward inhibition onto both subtypes of SPNs, and genetic disruption of mGluR5 in

488 parvalbumin interneurons increases striatum-dependent repetitive behaviors [40]. The
489 modulation of synaptic strength at these connections by fenobam and JNJ could also
490 partly account for the effects of these compounds on dSPN activity and behavior when
491 systemically administered, which would not occur in cKO animals.

492 Collateral inhibition between SPNs is another potential source for modulation of
493 co-activity. *In vitro* electrophysiology has shown that dSPNs are more likely to form
494 synapses onto other dSPNs, while iSPNs form synapses onto neurons of both
495 pathways with equal probability [35]. However, the strength of collateral synapses formed
496 by dSPNs appears to be smaller than that of synapses formed by iSPNs. Our analysis
497 of iSPN activity in cKO mice suggests that iSPN circuit properties are largely normal
498 when mGluR5 is genetically disrupted in dSPNs, perhaps reflecting the less substantial
499 modulation of iSPN circuitry by dSPNs reported in the striatum, at least during
500 spontaneous behavior. Whether this relationship holds across additional behavioral
501 states remains to be addressed. Additionally, whether disruption of iSPN networks
502 affects dSPN networks, perhaps due to stronger unidirectional iSPN-dSPN connectivity,
503 is a key question for further research.

504 *Translation implications of dSPN spatiotemporal dynamics*

505 The relationship of mGluR5 pharmacology to dSPN spatial coordination and motor
506 output is clinically relevant to the treatment of motor disorders. Prior studies examining
507 the spatial coordination of SPNs in parkinsonian mice demonstrated that, following
508 dopamine depletion to model a parkinsonian state, dSPN activity was reduced but
509 maintained spatial coordination [11]. However, when levodopa induced dyskinesia (LID)
510 was modelled in these animals, dSPNs lost spatial coordination. In the current work, we
511 show that pharmacological inhibition of mGluR5 increases spatial coordination. It is
512 tempting to speculate, therefore, that in the case of LID, the therapeutic efficacy of
513 mGluR5 NAMs may involve regulation of the spatially coordinated co-activity of dSPNs.
514 Additionally, further examination of how spatially coordinated SPN activity is disrupted in
515 motor diseases involving basal ganglia pathology, may be a promising avenue for future
516 therapeutic development.

517 In summary our data demonstrate that the modulation of signaling that affects
518 synaptic properties of excitatory synapses onto dSPNs is a key mediator of the normal
519 patterns of SPN co-activity that typify the striatum's neural ensemble dynamics in
520 relation to spontaneous movement. These results provide further support for models
521 where the local synchronization of SPNs (and the basal ganglia circuit in general) is a
522 stronger determinant of motor output than their overall levels of activity. Our results also
523 provide a framework for future lines of inquiry to address how striatal synaptic properties
524 shape circuit function and striatum-dependent behavior.

525 **Methods:**

526 *Mice*

527 Animals were group housed with 14-hr:10-hr Light/Dark cycle and food and water were
528 provided ad libitum. Mice of both sexes, between 4-12 months old, were used and all
529 experiments were performed in accordance with procedures approved by the
530 Northwestern University IACUC. To express GCaMP6f in dSPNs we used mice
531 expressing Cre recombinase under the control of the drd1a promoter (D1cre, Drd1a-Cre
532 Ey262) [41]. A Cre-dependent GCaMP6f under the control of the synapsin promoter
533 (pAAV.Syn.Flex.GCaMP6f.WPRE.SV40, 100833-AAV9 from Addgene) was used for
534 delivery of the construct. For in vitro patch clamp electrophysiology experiments we
535 further crossed the D1Cre line to mice expressing a Cre-dependent tdTomato reporter
536 inserted in the *Gt26Sor* (Rosa26) locus (Ai9), in order to identify dSPNs in the DLS [42].
537 For genetic deletion of mGluR5 we used floxed mGluR5 mice (mGluR5$^{loxP/loxP}$) [32]
538 crossed to either D1cre mice (D1cre; mGluR5$^{f/f}$) for in vivo imaging experiments, or D1
539 cre mice crossed with Ai9 mice (D1cre; mGluR5$^{f/f}$; Ai9$^{+/+}$) for patch clamp experiments.
540 All mice were maintained on the C57BL6/J background strain.

541 Behavioral analysis

542 *Motor learning on the accelerating rotarod:*

543 Mice of both sexes were placed on the rotarod and the initial revolution speed set to 4
544 rpm for 120 s. The rotarod then accelerated at a rate of 0.12 rpm·s^{-1} for 300 s. Mice

545 were trained in three trials per day with a 30 min inter-trial interval for four consecutive
546 days (12 trials total).

547 *Open Field:*

548 The dimensions of the square open field arena (in cm) were 60 l × 60 w × 30 h .
549 Animals were placed in the middle of the arena at the start of the test and remained in
550 the arena for 30 min during which time their position was tracked using an overhead
551 camera and analyzed using software (Limelight; Actimetrics).

552 *Digging behavior:*

553 Mice were placed in a novel cage containing wood chip bedding (3-cm deep) in a
554 brightly lit, open area. Animals remained in the testing cage for 15 min. Mouse digging
555 time was manually scored using a stopwatch.

556 *Voluntary Wheel Running:*

557 Mice of either sex were single-housed with wireless running wheels (MedAssociates) for
558 at least 7 days. Total distance run was quantified for each day.

559 *Virus Injection:*

560 For mice that received a viral injection (pAAV.Syn.Flex.GCaMP6f.WPRE.SV40,
561 100833-AAV9 from Addgene) prior to GRIN lens implant, we anesthetized mice with
562 isoflurane (2% in O_2) and stereotaxically injected virus at a rate of 250 nl min^{-1} into the
563 DLS using a microsyringe with a 28-gauge beveled-tip needle (Hamilton Company,
564 Reno, NV). Stock titer virus was diluted 1:10 with sterile PBS. The coordinates for
565 injection were: A/P +/- 0.05 mm, M/L +/- 1.8 mm, D/V -2.4mm (from dura). For all DV
566 coordinates, we went 0.1 mm past the injection target and then withdrew the syringe
567 back to the target for the injection. After each injection, we left the syringe in place for
568 10 minutes and then slowly withdrew the syringe. We then sutured the scalp, injected
569 analgesic (Buprenorphine SR, 1 mg kg^{-1}), as well as meloxicam (2x / day for 48 hours, 5
570 mg·kg^{-1}), and allowed the mice to recover for at least 14 days.

571 *Silk fibroin coating of GRIN lenses:*

572 For animals in which we implanted a GRIN lens coated with a fibroin:AAV mixture, we
573 autoclaved both GRIN lenses, and a small aliquot of 5% W/V silk fibroin solution, prior
574 to coating. Then, the sterile fibroin solution was mixed 1:1 with stock titer AAV
575 (pAAV.Syn.Flex.GCaMP6f.WPRE.SV40, 100833-AAV9 from Addgene). A microsyringe
576 with a 23 gauge flat tip needle (Hamilton Company, Reno, NV) with a manual
577 stereotaxic injector (Stoelting) was used to apply a 1μL droplet of the mixture to the tip
578 of the GRIN lens in a biological safety cabinet. The mixture was allowed to dry slightly
579 for 5 minutes with the droplet in contact with both the GRIN lens surface and the syringe
580 needle tip before the syringe needle was removed, this prevented the mixture from
581 coating the side of the lens. Once the needle was removed the droplet was allowed to
582 fully dry to the surface of the lens for at least 1 hour before implanting. Lenses were
583 stored at 4°C for implanting either the same day or within approximately 24 hours.

584 *Surgical implantation of GRIN lens and viral transduction:*

585 Mice were anesthetized with isoflurane in O_2 (induction 4%; maintenance 2–3%).
586 Following verification of anesthesia, hair was trimmed from the incision site, the scalp
587 cleaned with three alternating swabs of betadine and 70% ethanol, and an incision
588 made through the scalp to uncover the skull. The skull surface was cleaned and verified
589 to be level by measuring the coordinates of bregma, lambda, and two sites +/- 2mm
590 lateral to the midline. The M/L and A/P coordinates for implantation of the GRIN lens
591 were marked on the skull (A/P +/- 0.05 mm, M/L +/- 2 mm) and a Dremel with a
592 sterilized 0.6-mm tip was used to remove an approximately 2-mm circular region around
593 the implant site. The skull was cleaned, dried, and scored crosswise with a scalpel.
594 While continuously perfusing the tissue with ACSF, the dura and cortex were removed
595 using a 26 GA blunt-end needle connected to a vacuum line until the fibers of the
596 corpus callosum became visible, at which point a 30 GA blunt-end needle was used to
597 carefully remove the fibers of the callosum until striatal tissue became visible under a
598 dissecting microscope. A 1-mm or 1.8-mm diameter GRIN lens was then lowered into
599 the aspiration site (D/V -2.4 mm), held in place using a pipette tip and vacuum line
600 attached to the stereotax. The lens was secured to the skull using dental cement
601 (Metabond) and cyanoacrylate glue. Buprenorphine SR, (1 $mg \cdot kg^{-1}$) was administered

602 following surgery, as well as meloxicam (2x / day for 48 hours, 5 $mg \cdot kg^{-1}$),
603 dexamethasone (1x / day, 0.2 $mg \cdot kg^{-1}$for 7 days), and Sulfatrim (for 7 days in the
604 drinking water). Mice were allowed to recover for 2–4 weeks before mounting the
605 miniature microscope.

606 *Miniscope Mounting and Imaging:*

607 Two-to-four weeks following surgery to implant the GRIN lens, the mouse was again
608 anesthetized under the stereotax and a miniscope (UCLA V3 or V4) with a baseplate
609 attached was lowered to the top focal plane of the GRIN lens. Once the optimal imaging
610 plane was found, the baseplate was secured with dental cement (Metabond, Parkell).

611 *In vivo Ca^{2+} imaging and Analysis:*

612 All mice were habituated to the weight of the miniscope over a 60-minute session in the
613 open field. Following habituation, we placed mice in the open field for 60 minutes each
614 day for 1-3 days with the miniscope attached. For analysis of calcium dynamics in dSPN
615 cKO mice, we analyzed data from the first 20 minutes of day 1 of these sessions. In the
616 majority of animals used in these experiments, we used v3 miniscopes which required
617 higher LED intensities compared to v4 miniscopes. Therefore, we limited recording to
618 20 minutes to limit photobleaching. For experiments testing fenobam, JZL and JNJ, 60
619 minutes of open field activity were recorded following IP injection. For these
620 experiments we used v4 scopes which allowed for the use of lower LED intensities.
621 Fenobam (26 mg/kg) and JZL (10 mg/kg) were administered immediately prior to the
622 test, following a 15-minute habituation. Due to its pharmacokinetics, JNJ was
623 administered 30 minutes prior to beginning the test. Fenobam was diluted in 40% beta-
624 cyclodextrin, 10% DMSO, JZL and JNJ were diluted in 10% DMSO and 90% corn oil.

625 We used open source V3 and V4 miniscopes (https://github.com/Aharoni-
626 Lab/Miniscope-v4) that were connected to a coaxial cable which connected to a
627 miniscope data acquisition board (DAQ) 3.3. The DAQ was connected to a computer via
628 a USB 3.0 cable. Data was collected via the Miniscope QT Software
629 (https://github.com/Aharoni-Lab/Miniscope-DAQ-QT-Software) at 20 frames per second.
630 Simultaneous video recordings of behavior were performed at approximately 30 fps,

631 and data was aligned posthoc using the time stamps collected by the miniscope
632 software for each frame. Miniscopes and DAQ boards were purchased from Open
633 Ephys, LabMaker, or parts were machined by Shylo Steitler (UCLA) and assembled.

634 *Pre-processing and motion correction:*

635 Videos were preprocessed to remove sensor noise using a 2D FFT spatial frequency
636 filter and lowpass butterworth filter (https://github.com/Aharoni-Lab/Miniscope-
637 v4/tree/master/Miniscope-v4-Denoising-Notebook) and then motion correction was
638 performed using the normcorr algorithm in the CaImAn package [43].

639 *Identification of neurons (CNMF-E):*

640 Cells were automatically identified using the CNMF-E algorithm [44]. Recordings were
641 grouped in batches of 1-5000 frames for processing, and spatially downsampled 2x
642 during running of the CNMF-E algorithm. The maximum neuron diameter was
643 determined based on manual observation of each of the motion corrected videos in
644 ImageJ and the minimum local correlation value (Cn) and signal to noise ratio (SNR) for
645 a pixel to be used as a cell "seed" was determined by visualizing the correlation image
646 for a subset of recording frames of each video. The threshold for merging neurons was
647 set at 0.65, neurons were merged if their distances were smaller than two pixels and
648 they had highly correlated spatial shapes (correlation >0.8) and small temporal
649 correlations (correlation <0.4). The output of the CNMF-E analysis performed on the
650 video was then manually checked to ensure accuracy.

651 *Analysis of Ca^{2+} activity:*

652 The cell Ca^{2+} activity traces from CNMF-E were processed first by scaling to the 99-
653 percentile value of each cell's activity trace during the recording session. The resulting
654 normalized trace was then expressed as a Z-score by subtracting each sample from the
655 mean and dividing by the standard deviation of the entire trace. Finally, this trace was
656 downsampled to 5Hz (using the maximum value within the down sampled regions) and
657 this result was used for further analysis.

658 *Ca^{2+} event rate and correlation to velocity:*

A threshold crossing algorithm was used to detect peaks that were ≥2.5 s.d. above the baseline signal value for 1 second and the time of each event was calculated as the midpoint between the maximum value of the event and the preceding minimum [11]. We used EZ track [45] to compute the frame by frame velocity of the animal in the openfield arena. Using custom Python scripts we applied a 1 second median filter to this velocity trace and downsampled to 5Hz for alignment to the Ca^{2+} activity data.

Pairwise cell co-activity:

The Jaccard index of pairwise coactivity was calculated following 1 second "forward-smoothing" of the Ca^{2+} activity traces as described previously [11]. The mean value of the Jaccard index was calculated as a function of the Euclidean distance between cells in a neuron pair and the mean values were binned into either 50 or 250 μm bins. These values were normalized to shuffled data sets where the Ca^{2+} traces for each cell were shuffled in time, using 1,000 independent shuffles of the binarized Ca^{2+} event traces for each cell. This data was used for statistical comparison of coactivity between groups as a function of distance, and behavioral state, i.e. moving or resting.

Spatial coordination index

To measure spatial coordination, the extent to which co-activity is greater among more proximal neurons versus more distal cells, during each frame of the video we calculated a previously used metric, the spatial coordination index (SCI) [11]. For each frame of the down-sampled video, we shuffled the pairwise distances for each neuron pair (1000 independent shuffles for each frame of the video), but not each cell's Ca^{2+} activity signal. From these 1000 different distributions of distances between cell pairs, we calculated the cumulative distribution of active cell distances for the actual dataset and each shuffled dataset. We then performed a pair of Kolmogorov–Smirnov tests to determine if the cumulative distribution of active cell distances in each frame was smaller (i.e. left shifted or more "clustered") or greater (right-shifted or less "clustered") than that of the shuffled data. We took the logarithm (base ten) of the smaller p value from either test and used this value as the spatial coordination index. If a frame did not have any active cell pairs the index is 0. This analysis allows for visualization of how spatiotemporal dynamics change more specifically during movement onset.

689 *Detection of movement onset*

690 To most precisely detect instances of movement onset, specifically forward ambulatory
691 motion, for our SCI analysis, we used the frame by frame velocity calculated from the
692 mouse's centroid location detected by ezTrack. We then filtered the velocity traces by
693 determining if the animal's centroid moved by more than 1cm from its location in the
694 current frame at any point over the next 1 second of the recording. If not, we set the
695 velocity to 0 for that frame. We then smoothed the resulting trace using a .167ms
696 moving average. To find periods of movement onset that would allow us to more clearly
697 measure whether there were consistent changes in spatial coordination, we identified
698 where this velocity trace exceeded 0.5cm/sec for at least 2 seconds preceded by a
699 period of rest for 4 seconds. We used the timestamps recorded by the miniscope
700 software to find the matching period in our SCI signal. This allowed us to clearly
701 measure how the degree of spatial coordination among dSPNs changes between rest
702 and movement.

703 *Slice procedure and in vitro Electrophysiological Recording:*

704 Parasagittal slices containing the dorsal striatum were prepared using standard
705 techniques. Mice were deeply anesthetized (xylazine 10mg/kg and ketamine 100mg/kg
706 i.p.) before undergoing transcardial perfusion with an ice-cold sucrose artificial
707 cerebrospinal fluid (ACSF) solution containing (in mM): 85 NaCl, 2.5 KCl, 1.25
708 NaH_2PO_4, 25 $NaHCO_3$, 25 glucose, 75 sucrose, 0.5 $CaCl_2$ and 4 $MgCl_2$, equilibrated
709 with 95% O_2 and 5% CO_2. The brain was removed and mounted on the stage of
710 vibratome (Leica Microsystems, Inc). 350 μm thick sections were made in ice-cold
711 sucrose ACSF. Slices were transferred to a recovery chamber containing the sucrose
712 slicing ACSF solution, which was gradually exchanged for a normal ACSF containing (in
713 mM): 125 NaCl, 2.4 KCl, 1.2 Na_2PO_4, 25 $NaHCO_3$, 25 glucose, 1 $CaCl_2$ and 2 $MgCl_2$,
714 while the slices were maintained at 30°C. Individual slices were transferred to a
715 recording chamber and visualized under DIC. Micro-Manager open source software was
716 used for collecting the CCD camera image [46]. For extracellular recordings, slices were
717 perfused with normal ACSF containing (in mM): 125 NaCl, 2.4 KCl, 1.2 Na_2PO_4, 25
718 $NaHCO_3$, 25 glucose, 2 $CaCl_2$ and 1 $MgCl_2$. Recording electrodes were manufactured

719 from borosilicate glass pipettes and had resistances of 3-5 MΩ when filled with regular
720 ACSF. For whole-cell voltage clamp experiments, recording electrodes were filled with
721 internal solution containing (in mM) 95 CsF, 25 CsCl, 10 Cs-HEPES, 10 Cs-EGTA, 2
722 NaCl, 2 Mg-ATP, 10 QX-314, 5 TEA-Cl, 5 4-AP for recording of EPSCs, or 75
723 $CsCH_3SO_3$, 60 CsCl, 1 $MgCl_2$, 0.2 EGTA, 10 HEPES, 2 Mg-ATP 0.3 GTP-Na_2, 10 Na_2-
724 phosphocreatine,10 TEA, 5 QX-314. Striatal projection neurons (SPNs) were visually
725 identified and were voltage clamped at -80mV. Miniature events (mEPSCs) were
726 recorded in the presence of the Na^+ channel blocker TTX (1μM) and bicuculline (10
727 μM). Analysis of mEPSCs was performed using Eventer software
728 (https://eventerneuro.netlify.app/).

729 *Histology:*

730 Following in vivo imaging experiments, mice were anesthetized using ketamine/xylazine
731 and perfused with PBS containing 0.02% sodium nitrite and 4 mM $MgSO_4$ followed by
732 2% paraformaldehyde in 0.1 M sodium acetate buffer (pH 6.5) for 6 min, and 2%
733 paraformaldehyde in 0.1 M sodium borate buffer (pH 8.5) for 12–18 min. The brains
734 were removed from the skull, post-fixed overnight in 2% paraformaldehyde in 0.1 M
735 sodium borate buffer (pH 8.5), then sectioned coronally at 50 μm on a Leica Vibratome
736 VT1000s in PBS. The sections were collected and stored at 4 °C in PBS containing
737 0.02% sodium azide. Free-floating sections were rinsed for 30 min in PBS followed by
738 four 15-min washes in PBS containing 0.1% Triton X-100 (Sigma, T8787) and 0.1%
739 bovine serum albumin (BSA; Sigma, A4503). The sections were then blocked with 3%
740 normal donkey serum (NDS; Jackson ImmunoResearch, 017-000-121) for 1 h and then
741 incubated in primary antibody overnight (Mouse anti-GFP, Millipore, MAB3580).
742 Sections were washed three times for 15 min and then incubated in secondary antibody
743 for 1 h and washed three times prior to mounting and imaging with a 20× objective on a
744 Nikon A1 confocal microscope. Z-series were taken with a 0.82 μm step size.

745 *Statistics:*

746 For comparisons of single mean values per mouse, for instance mean velocity per
747 animal, we used non-parametric Mann Whitney U test or the Wilcoxon Signed Rank
748 test. Where the same measurement was made multiple times, we used a repeated

measures ANOVA. For cases where multiple different but correlated, non-independent, comparisons were made within mice, for instance in comparing mean event rates at different speeds or mean coactivity across neuron pairs at difference distances, we used a linear mixed effects model (LMM) to account for the non-independence of measurements made from the same animal. The model was implemented using the statsmodels python package (https://www.statsmodels.org), the drug treatment or genotype was the independent variable, mean values measured per mouse are the dependent variables and individual mice are the group term. Where this model was used, we tested for the effect of genotype or drug treatment, and reported the significance for that measurement. In all figures, individual data points represent the mean of a group, and errors bars the standard error of the mean. N numbers for each group are specified in the figure legend.

References

1. Klaus, A., Alves da Silva, J., and Costa, R.M. (2019). What, If, and When to Move: Basal Ganglia Circuits and Self-Paced Action Initiation. Annu Rev Neurosci *42*, 459-483. 10.1146/annurev-neuro-072116-031033.
2. Wolff, S.B.E., Ko, R., and Olveczky, B.P. (2022). Distinct roles for motor cortical and thalamic inputs to striatum during motor skill learning and execution. Sci Adv *8*, eabk0231. 10.1126/sciadv.abk0231.
3. Dang, M.T., Yokoi, F., Yin, H.H., Lovinger, D.M., Wang, Y., and Li, Y. (2006). Disrupted motor learning and long-term synaptic plasticity in mice lacking NMDAR1 in the striatum. Proc Natl Acad Sci U S A *103*, 15254-15259. 10.1073/pnas.0601758103.
4. Rothwell, P.E., Hayton, S.J., Sun, G.L., Fuccillo, M.V., Lim, B.K., and Malenka, R.C. (2015). Input- and Output-Specific Regulation of Serial Order Performance by Corticostriatal Circuits. Neuron *88*, 345-356. 10.1016/j.neuron.2015.09.035.
5. Yin, H.H., Mulcare, S.P., Hilario, M.R., Clouse, E., Holloway, T., Davis, M.I., Hansson, A.C., Lovinger, D.M., and Costa, R.M. (2009). Dynamic reorganization of striatal circuits during the acquisition and consolidation of a skill. Nat Neurosci *12*, 333-341. 10.1038/nn.2261.
6. Hwang, F.J., Roth, R.H., Wu, Y.W., Sun, Y., Kwon, D.K., Liu, Y., and Ding, J.B. (2022). Motor learning selectively strengthens cortical and striatal synapses of motor engram neurons. Neuron *110*, 2790-2801 e2795. 10.1016/j.neuron.2022.06.006.
7. Gerfen, C.R., and Surmeier, D.J. (2011). Modulation of striatal projection systems by dopamine. Annu Rev Neurosci *34*, 441-466. 10.1146/annurev-neuro-061010-113641.

8. Nelson, A.B., and Kreitzer, A.C. (2014). Reassessing models of basal ganglia function and dysfunction. Annu Rev Neurosci *37*, 117-135. 10.1146/annurev-neuro-071013-013916.
9. Cui, G., Jun, S.B., Jin, X., Pham, M.D., Vogel, S.S., Lovinger, D.M., and Costa, R.M. (2013). Concurrent activation of striatal direct and indirect pathways during action initiation. Nature *494*, 238-242. 10.1038/nature11846.
10. Barbera, G., Liang, B., Zhang, L., Gerfen, C.R., Culurciello, E., Chen, R., Li, Y., and Lin, D.T. (2016). Spatially Compact Neural Clusters in the Dorsal Striatum Encode Locomotion Relevant Information. Neuron *92*, 202-213. 10.1016/j.neuron.2016.08.037.
11. Parker, J.G., Marshall, J.D., Ahanonu, B., Wu, Y.W., Kim, T.H., Grewe, B.F., Zhang, Y., Li, J.Z., Ding, J.B., Ehlers, M.D., and Schnitzer, M.J. (2018). Diametric neural ensemble dynamics in parkinsonian and dyskinetic states. Nature *557*, 177-182. 10.1038/s41586-018-0090-6.
12. Klaus, A., Martins, G.J., Paixao, V.B., Zhou, P., Paninski, L., and Costa, R.M. (2017). The Spatiotemporal Organization of the Striatum Encodes Action Space. Neuron *95*, 1171-1180 e1177. 10.1016/j.neuron.2017.08.015.
13. Yun, S., Yang, B., Anair, J.D., Martin, M.M., Fleps, S.W., Pamukcu, A., Yeh, N.H., Contractor, A., Kennedy, A., and Parker, J.G. (2023). Antipsychotic drug efficacy correlates with the modulation of D1 rather than D2 receptor-expressing striatal projection neurons. Nat Neurosci *26*, 1417-1428. 10.1038/s41593-023-01390-9.
14. Wilson, C.J., and Groves, P.M. (1981). Spontaneous firing patterns of identified spiny neurons in the rat neostriatum. Brain Res *220*, 67-80. 10.1016/0006-8993(81)90211-0.
15. Wilson, C.J., and Kawaguchi, Y. (1996). The origins of two-state spontaneous membrane potential fluctuations of neostriatal spiny neurons. J Neurosci *16*, 2397-2410. 10.1523/JNEUROSCI.16-07-02397.1996.
16. Guo, Q., Wang, D., He, X., Feng, Q., Lin, R., Xu, F., Fu, L., and Luo, M. (2015). Whole-brain mapping of inputs to projection neurons and cholinergic interneurons in the dorsal striatum. PLoS One *10*, e0123381. 10.1371/journal.pone.0123381.
17. Wall, N.R., De La Parra, M., Callaway, E.M., and Kreitzer, A.C. (2013). Differential innervation of direct- and indirect-pathway striatal projection neurons. Neuron *79*, 347-360. 10.1016/j.neuron.2013.05.014.
18. Wu, Y.W., Kim, J.I., Tawfik, V.L., Lalchandani, R.R., Scherrer, G., and Ding, J.B. (2015). Input- and cell-type-specific endocannabinoid-dependent LTD in the striatum. Cell Rep *10*, 75-87. 10.1016/j.celrep.2014.12.005.
19. Li, W., and Pozzo-Miller, L. (2020). Dysfunction of the corticostriatal pathway in autism spectrum disorders. J Neurosci Res *98*, 2130-2147. 10.1002/jnr.24560.
20. Surmeier, D.J., Plotkin, J., and Shen, W. (2009). Dopamine and synaptic plasticity in dorsal striatal circuits controlling action selection. Curr Opin Neurobiol *19*, 621-628. 10.1016/j.conb.2009.10.003.
21. Gerdeman, G.L., Ronesi, J., and Lovinger, D.M. (2002). Postsynaptic endocannabinoid release is critical to long-term depression in the striatum. Nat Neurosci *5*, 446-451. 10.1038/nn832.

22. Bagetta, V., Picconi, B., Marinucci, S., Sgobio, C., Pendolino, V., Ghiglieri, V., Fusco, F.R., Giampa, C., and Calabresi, P. (2011). Dopamine-dependent long-term depression is expressed in striatal spiny neurons of both direct and indirect pathways: implications for Parkinson's disease. J Neurosci *31*, 12513-12522. 10.1523/JNEUROSCI.2236-11.2011.
23. Kreitzer, A.C., and Malenka, R.C. (2007). Endocannabinoid-mediated rescue of striatal LTD and motor deficits in Parkinson's disease models. Nature *445*, 643-647. 10.1038/nature05506.
24. Marshall, J.J., Xu, J., and Contractor, A. (2018). Kainate Receptors Inhibit Glutamate Release Via Mobilization of Endocannabinoids in Striatal Direct Pathway Spiny Projection Neurons. J Neurosci *38*, 3901-3910. 10.1523/JNEUROSCI.1788-17.2018.
25. Chevaleyre, V., Takahashi, K.A., and Castillo, P.E. (2006). Endocannabinoid-mediated synaptic plasticity in the CNS. Annu Rev Neurosci *29*, 37-76. 10.1146/annurev.neuro.29.051605.112834.
26. Jackman, S.L., Chen, C.H., Chettih, S.N., Neufeld, S.Q., Drew, I.R., Agba, C.K., Flaquer, I., Stefano, A.N., Kennedy, T.J., Belinsky, J.E., et al. (2018). Silk Fibroin Films Facilitate Single-Step Targeted Expression of Optogenetic Proteins. Cell Rep *22*, 3351-3361. 10.1016/j.celrep.2018.02.081.
27. Aharoni, D., and Hoogland, T.M. (2019). Circuit Investigations With Open-Source Miniaturized Microscopes: Past, Present and Future. Front Cell Neurosci *13*, 141. 10.3389/fncel.2019.00141.
28. Shin, J.H., Song, M., Paik, S.B., and Jung, M.W. (2020). Spatial organization of functional clusters representing reward and movement information in the striatal direct and indirect pathways. Proc Natl Acad Sci U S A *117*, 27004-27015. 10.1073/pnas.2010361117.
29. Uchigashima, M., Narushima, M., Fukaya, M., Katona, I., Kano, M., and Watanabe, M. (2007). Subcellular arrangement of molecules for 2-arachidonoyl-glycerol-mediated retrograde signaling and its physiological contribution to synaptic modulation in the striatum. J Neurosci *27*, 3663-3676. 10.1523/JNEUROSCI.0448-07.2007.
30. Xu, J., Marshall, J.J., Kraniotis, S., Nomura, T., Zhu, Y., and Contractor, A. (2021). Genetic disruption of Grm5 causes complex alterations in motor activity, anxiety and social behaviors. Behav Brain Res *411*, 113378. 10.1016/j.bbr.2021.113378.
31. Conde-Ceide, S., Martinez-Viturro, C.M., Alcazar, J., Garcia-Barrantes, P.M., Lavreysen, H., Mackie, C., Vinson, P.N., Rook, J.M., Bridges, T.M., Daniels, J.S., et al. (2015). Discovery of VU0409551/JNJ-46778212: An mGlu5 Positive Allosteric Modulator Clinical Candidate Targeting Schizophrenia. ACS Med Chem Lett *6*, 716-720. 10.1021/acsmedchemlett.5b00181.
32. Xu, J., Zhu, Y., Contractor, A., and Heinemann, S.F. (2009). mGluR5 has a critical role in inhibitory learning. J Neurosci *29*, 3676-3684. 10.1523/JNEUROSCI.5716-08.2009.
33. Gerfen, C.R., Paletzki, R., and Heintz, N. (2013). GENSAT BAC cre-recombinase driver lines to study the functional organization of cerebral cortical and basal ganglia circuits. Neuron *80*, 1368-1383. 10.1016/j.neuron.2013.10.016.

34. Madisen, L., Zwingman, T.A., Sunkin, S.M., Oh, S.W., Zariwala, H.A., Gu, H., Ng, L.L., Palmiter, R.D., Hawrylycz, M.J., Jones, A.R., et al. (2010). A robust and high-throughput Cre reporting and characterization system for the whole mouse brain. Nat Neurosci *13*, 133-140. 10.1038/nn.2467.
35. Taverna, S., Ilijic, E., and Surmeier, D.J. (2008). Recurrent collateral connections of striatal medium spiny neurons are disrupted in models of Parkinson's disease. J Neurosci *28*, 5504-5512. 10.1523/JNEUROSCI.5493-07.2008.
36. Saunders, A., Johnson, C.A., and Sabatini, B.L. (2012). Novel recombinant adeno-associated viruses for Cre activated and inactivated transgene expression in neurons. Front Neural Circuits *6*, 47. 10.3389/fncir.2012.00047.
37. McElvain, L.E., Chen, Y., Moore, J.D., Brigidi, G.S., Bloodgood, B.L., Lim, B.K., Costa, R.M., and Kleinfeld, D. (2021). Specific populations of basal ganglia output neurons target distinct brain stem areas while collateralizing throughout the diencephalon. Neuron *109*, 1721-1738 e1724. 10.1016/j.neuron.2021.03.017.
38. Parent, A., and De Bellefeuille, L. (1982). Organization of efferent projections from the internal segment of globus pallidus in primate as revealed by fluorescence retrograde labeling method. Brain Res *245*, 201-213. 10.1016/0006-8993(82)90802-2.
39. Shen, W., Plotkin, J.L., Francardo, V., Ko, W.K., Xie, Z., Li, Q., Fieblinger, T., Wess, J., Neubig, R.R., Lindsley, C.W., et al. (2015). M4 Muscarinic Receptor Signaling Ameliorates Striatal Plasticity Deficits in Models of L-DOPA-Induced Dyskinesia. Neuron *88*, 762-773. 10.1016/j.neuron.2015.10.039.
40. Barnes, S.A., Pinto-Duarte, A., Kappe, A., Zembrzycki, A., Metzler, A., Mukamel, E.A., Lucero, J., Wang, X., Sejnowski, T.J., Markou, A., and Behrens, M.M. (2015). Disruption of mGluR5 in parvalbumin-positive interneurons induces core features of neurodevelopmental disorders. Mol Psychiatry *20*, 1161-1172. 10.1038/mp.2015.113.
41. Gong, S., Doughty, M., Harbaugh, C.R., Cummins, A., Hatten, M.E., Heintz, N., and Gerfen, C.R. (2007). Targeting Cre Recombinase to Specific Neuron Populations with Bacterial Artificial Chromosome Constructs. The Journal of Neuroscience *27*, 9817-9823.
42. Madisen, L., Zwingman, T.A., Sunkin, S.M., Oh, S.W., Zariwala, H.A., Gu, H., Ng, L.L., Palmiter, R.D., Hawrylycz, M.J., Jones, A.R., et al. (2010). A robust and high-throughput Cre reporting and characterization system for the whole mouse brain. Nature neuroscience *13*, 133-140. 10.1038/nn.2467.
43. Giovannucci, A., Friedrich, J., Gunn, P., Kalfon, J., Brown, B.L., Koay, S.A., Taxidis, J., Najafi, F., Gauthier, J.L., Zhou, P., et al. (2019). CaImAn an open source tool for scalable calcium imaging data analysis. Elife *8*. 10.7554/eLife.38173.
44. Zhou, P., Resendez, S.L., Rodriguez-Romaguera, J., Jimenez, J.C., Neufeld, S.Q., Giovannucci, A., Friedrich, J., Pnevmatikakis, E.A., Stuber, G.D., Hen, R., et al. (2018). Efficient and accurate extraction of in vivo calcium signals from microendoscopic video data. Elife *7*. 10.7554/eLife.28728.
45. Pennington, Z.T., Diego, K.S., Francisco, T.R., LaBanca, A.R., Lamsifer, S.I., Liobimova, O., Shuman, T., and Cai, D.J. (2021). ezTrack-A Step-by-Step Guide to Behavior Tracking. Curr Protoc *1*, e255. 10.1002/cpz1.255.

46. Edelstein, A.D., Tsuchida, M.A., Amodaj, N., Pinkard, H., Vale, R.D., and Stuurman, N. (2014). Advanced methods of microscope control using muManager software. J Biol Methods *1*. 10.14440/jbm.2014.36.

Acknowledgments

The authors thank Dr. Craig Weiss and Northwestern University behavioral phenotyping core facility for technical support.

Funding:

This work was supported by NIH R01 MH099114 to AC

Author contributions:

Conceptualization: JJM, JX, JGP, AC
Methodology: JJM, JX, JGP, AC
Investigation: JJM, JX, NHY, SY, TN, JA
Visualization: JJM, JGP, AC
Supervision: JJM, JGP, AC
Writing—original draft: JJM, AC
Writing—review & editing: JJM, AC, JGP

Competing interests:

The authors declare that they have no competing interests.

Data and materials availability:

All data needed to evaluate the conclusions in the paper are present in the paper and/or the Supplementary Materials. Code and summary data needed to replicate figures in the paper will be made publicly available in an archival database prior to the date of publication.

Figures and legends:

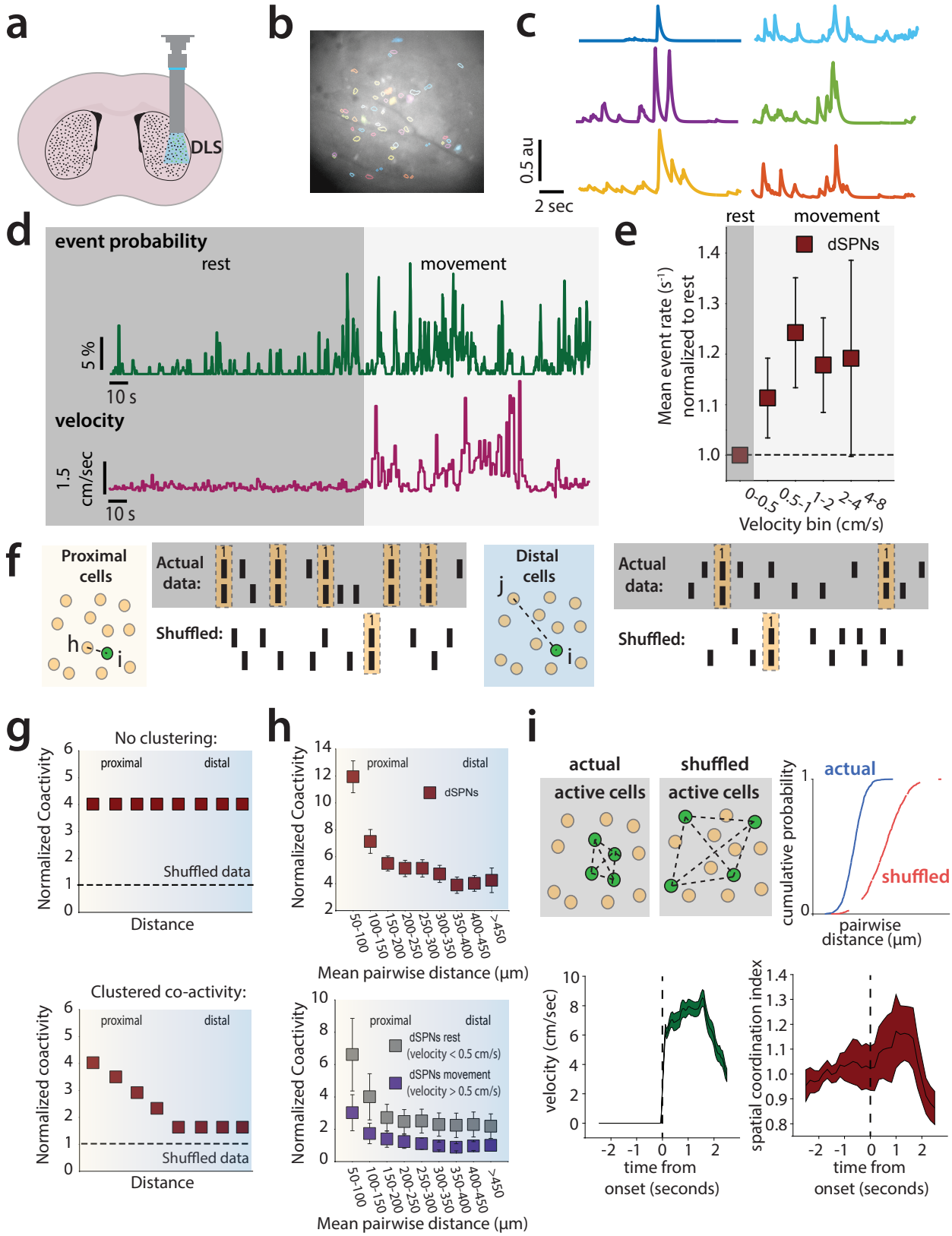

948

949 **Figure 1) dSPNs exhibit spatially clustered activity that varies with movement**

950 (**a**) Cartoon representation of implanted GRIN lens and miniscope imaging in the DLS.
951 (**b**) Examples of segmented cell outlines from the CNMF-E algorithm in a single mouse.
952 (**c**) Example of Ca^{2+} traces from corresponding colored and filled segmented cells
953 shown in (b). (**d**) The probability of a Ca^{2+} event in detected cells increases during
954 movement in dSPNs. (**e**) The Ca^{2+} event rate in detected cells increases during
955 movement in dSPNs ($p=0.240$, Wilcoxon Signed Rank Test, events/second during bins
956 with velocity>0.5 cm/sec vs. during bins with velocity<0.5 cm/sec). (**f**) Cartoon
957 schematic to illustrate analysis of co-activity as a function of distance between cell pairs.
958 Across all cell pairs in the field-of-view for each session, a correlation matrix was
959 generated, in which, for each frame of the recording, the cell pair was scored a 1 if both
960 cells were active, or 0 otherwise. These scores for each frame were averaged across all
961 frames in the recording, to generate an average co-activity score for that pair. Then,
962 those values were normalized to averages measured from independently shuffled Ca^{2+}
963 traces for each cell in the recording (using 1000 independent shuffles for each cell
964 trace), to control for changes in mean activity level between conditions. (**g**) Hypothetical
965 plot of shuffle-normalized jaccard scores versus distance when coactivity is not
966 "clustered" and hypothetical plot of "clustered" co-activity. Co-activity decreases during
967 periods of movement (Linear Mixed Effects Model/LMM, $p<0.000$, $z=-4.852$, $\beta=-1.671$,
968 SE = 0.344, 95% CI: [-2.346 -0.996] , N=5 mice). **(i)** The spatial coordination index (SCI)
969 peaks during movement onset ($p<0.000$, $z=12.21$, Wilcoxon Signed Rank Test,
970 comparing the peak value of the normalized SCI during 2.5 seconds following
971 movement onset to 1).

972

973
974

975 **Figure 1 – supplementary data 1**
976

Mouse	Total Cells	Sessions
19.2	318	5
1.2	78	2
20.2	311	2
24.2	20	2
25.2	307	4
26.2	176	2
2.7	136	3

977
978 **Table 1)** Number of cells per animal and recording sessions from animals used in figure
979 1 analysis
980
981

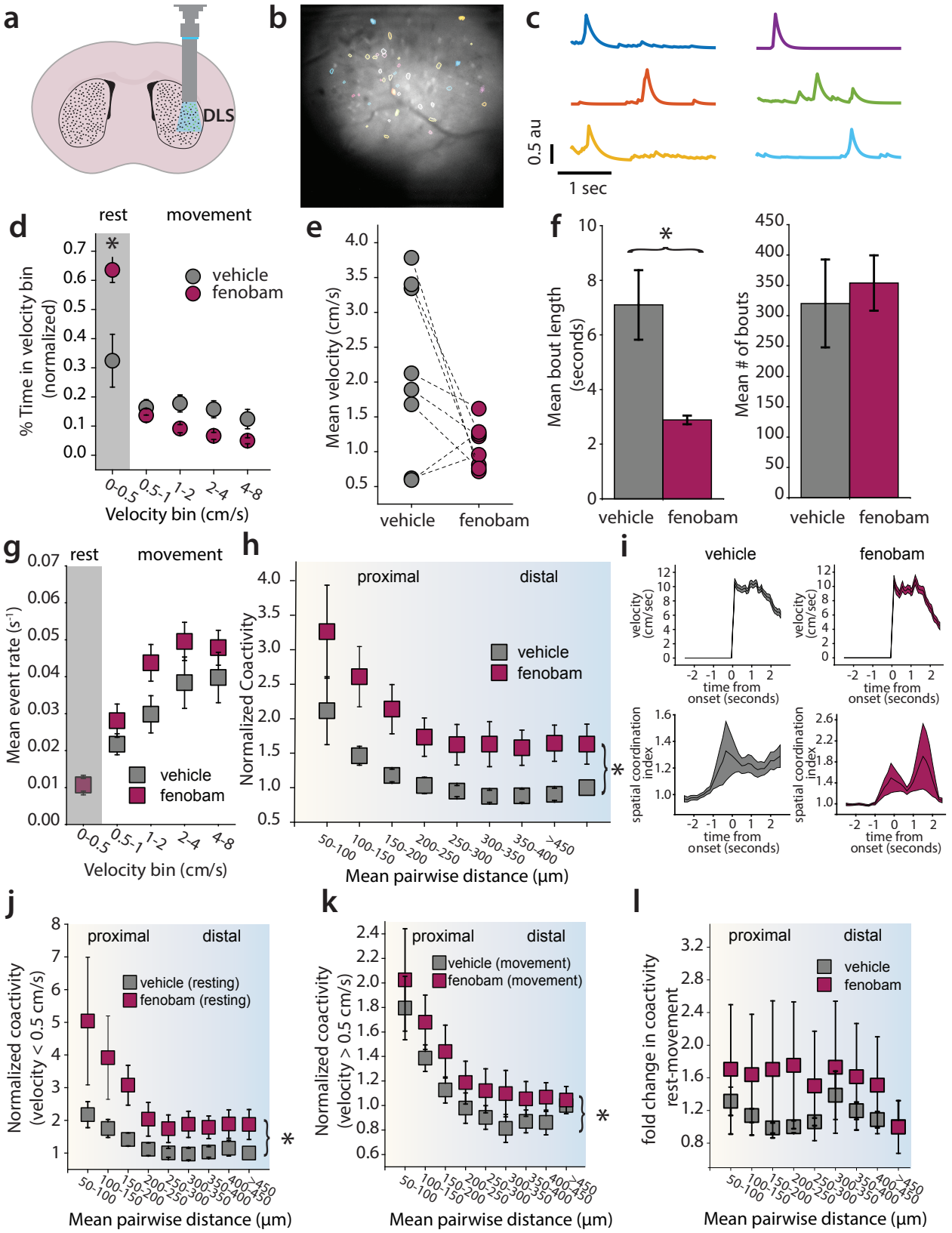
a
DLS
b
c
0.5 au
1 sec
d
rest
movement
% Time in velocity bin (normalized)
vehicle
fenobam
Velocity bin (cm/s)
e
Mean velocity (cm/s)
vehicle
fenobam
f
Mean bout length (seconds)
Mean # of bouts
g
Mean event rate (s⁻¹)
h
proximal
distal
Normalized Coactivity
Mean pairwise distance (μm)
i
vehicle
fenobam
velocity (cm/sec)
time from onset (seconds)
spatial coordination index
j
Normalized coactivity (velocity < 0.5 cm/s)
vehicle (resting)
fenobam (resting)
k
Normalized coactivity (velocity > 0.5 cm/s)
vehicle (movement)
fenobam (movement)
l
fold change in coactivity rest-movement

982

983 **Figure 2) A negative allosteric modulator of mGluR5 increases coactivity among**
984 **dSPN pairs**(**a**) Cartoon representing implanted GRIN lens and miniscope imaging in the
985 DLS (**b**) Examples of segmented cell outlines from the CNMF-E algorithm in a single
986 mouse. (**c**) Example of Ca^{2+} traces from corresponding filled segmented cells shown in
987 (b) (**d**) Binned velocity of animal. Fenobam increased the amount of time the animal
988 spends at rest (Vehicle mean: 0.324 ± 0.091, fenobam mean: 0.635 ± 0.043, p=0.024,
989 U=10, Mann-Whitney U test) (**e**) Mean velocity of animals following vehicle or fenobam
990 treatment. The fenobam effect on mean velocity during the open field test is not
991 significant (Mann-Whitney U test, p=0.103, U=48) (**f**) Mean bout length of animals
992 during vehicle or fenobam. Fenobam reduces the mean bout length (Vehicle: 7.098
993 seconds ± 1.272, Fenobam: 2.886 seconds ± 0.160, Mann-Whitney U test, p<0.001,
994 U=0), but does not affect the number of bouts (Mann-Whitney U test, p=0.793, U=35).
995 (**g**) The average event rate of dSPNs at each movement velocity of the mouse. This
996 relationship is not affected by fenobam administration (Linear Mixed Effects
997 Model/LMM, p=0.754, z=-0.313, β=-0.002, SE = 0.006, 95% CI: [-0.014 0.010] , N=8
998 mice). (**h**) Fenobam increases the pairwise coactivity of dSPNs when grouped into 50
999 µm bins (LMM, p<0.000, z=-6.050, β=-0.828, SE = 0.137, 95% CI: [-1.096 -0.560] , N=8
1000 mice) **(i)** Following both vehicle and drug treatment spatial coordination peaks during
1001 movement onset (Veh: p<0.000, z=12.21, Drug: p<0.000, z=10.1804) (**j**) Pairwise
1002 coactivity during rest with vehicle and fenobam treatment (velocity <0.5 $cm*sec^{-1}$)(LMM,
1003 p<0.000, z=-4.448, β=-1.292, SE = 0.290, 95% CI: [-1.861 -0.723] , N=8 mice) (**k**)
1004 Pairwise coactivity during movement (velocity >0.5 $cm*sec^{-1}$) with vehicle and fenobam
1005 (LMM, p=0.008, z=-2.673, β=-0.220, SE = 0.082, 95% CI: [-0.381 -0.059] , N=8 mice)
1006 (**l**) Fenobam does not affect the relative decrease in coactivity seen during movement

1007
1008
1009
1010
1011
1012
1013

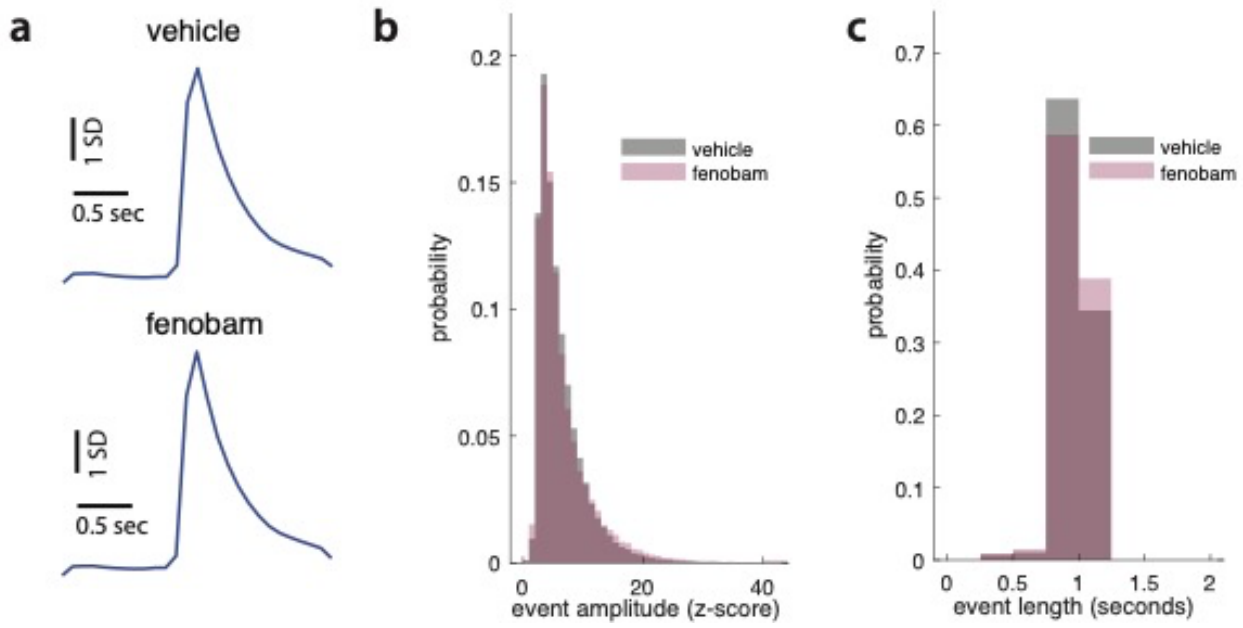

Figure 2 supplementary data 1

a) Averaged Ca^{2+} transients from vehicle and fenobam treated mice **b)** Fenobam treatment does not affect the distribution of event amplitudes (LMM, p=0.246, z=-1.160, β=-0.555, SE=0.478, 95% CI: [-1.493 0.383], N=8 mice) **c**) Fenobam treatment does not affect the distribution of event lengths (LMM, p=0.499, z=-0.676, β=-0.044, SE=0.065, 95% CI: [-0.173 0.084], N=8 mice)

1036 **Figure 2 – supplementary data 2**

1037

1038 Vehicle sessions for fenobam experiments

Mouse	Cells	Sessions
2.7	96	2
2.8	40	2
2.14	58	2
m974	293	1
m973	277	1
f979	164	1
f977	136	1
f976	387	1

1039

1040 Fenobam sessions

Mouse	Cells	Sessions
2.7	100	2
2.8	41	2
2.14	84	1
m974	91	1
m973	191	1
f979	29	1
f977	157	1
f976	219	1

1041

1042

1043 **Table 2)** Number of cells per animal and recording sessions from animals used in figure
1044 2 analysis

1045

1046

1047

1048

1049

1050

1051

1052

1053

1054

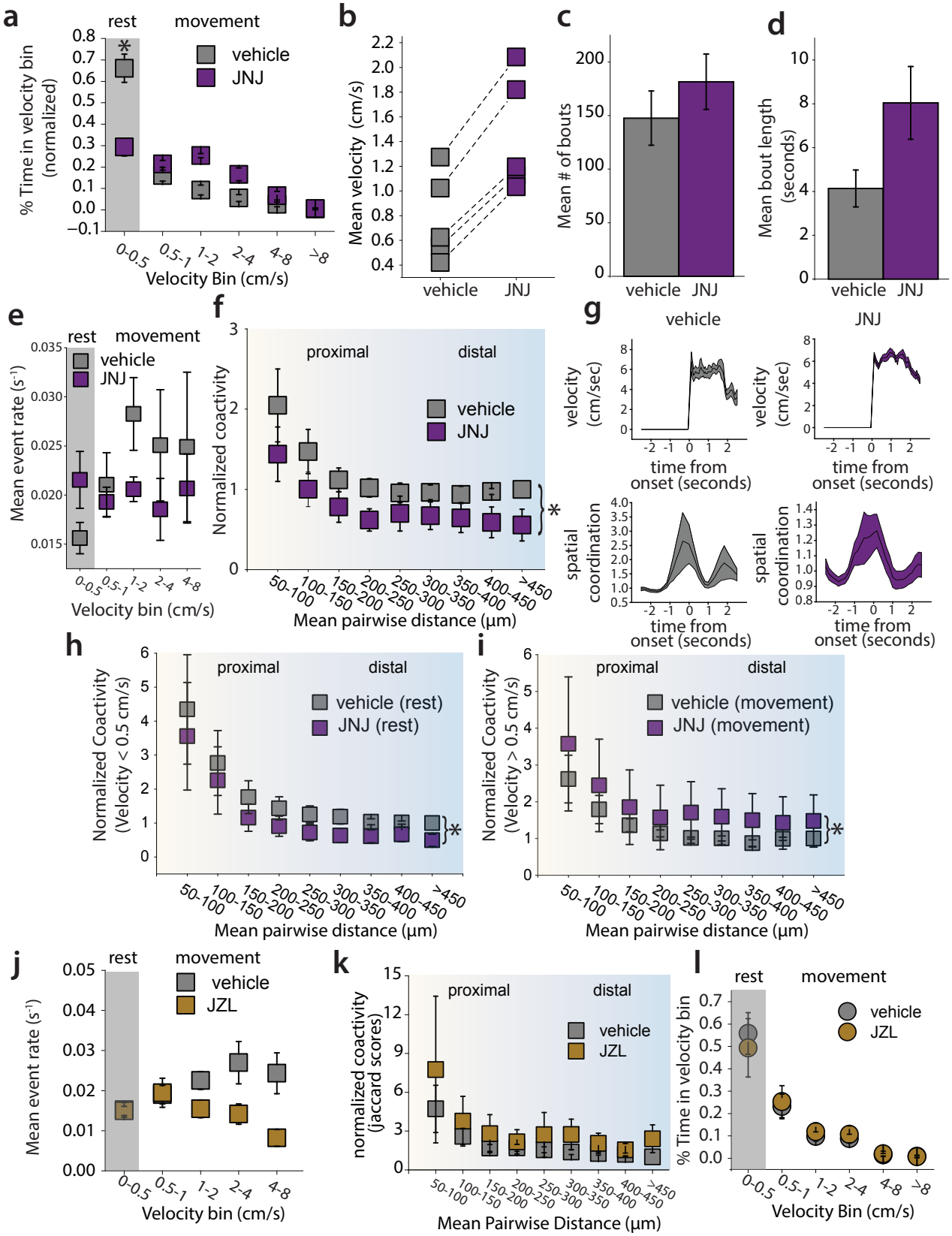
a
rest
movement
vehicle
JNJ
% Time in velocity bin (normalized)
Velocity Bin (cm/s)
0-0.5
0.5-1
1-2
2-4
4-8
>8
b
Mean velocity (cm/s)
vehicle
JNJ
c
Mean # of bouts
d
Mean bout length (seconds)
e
Mean event rate (s⁻¹)
Velocity bin (cm/s)
f
proximal
distal
Normalized coactivity
Mean pairwise distance (µm)
50-100
100-150
150-200
200-250
250-300
300-350
350-400
400-450
>450
g
velocity (cm/sec)
time from onset (seconds)
spatial coordination
h
Normalized Coactivity (Velocity < 0.5 cm/s)
vehicle (rest)
JNJ (rest)
i
Normalized Coactivity (Velocity > 0.5 cm/s)
vehicle (movement)
JNJ (movement)
j
JZL
k
normalized coactivity (jaccard scores)
Mean Pairwise Distance (µm)
l

1055

Figure 3) A positive allosteric modulator of mGluR5, JNJ-46778212, decreases clustered coactivity of dSPNs

(**a**) Time animal spent in each velocity bin and (**b**) Mean velocity of the animals during vehicle and after JNJ administration. JNJ decreases the amount of time the animal spends at rest (Vehicle mean: 0.661 ± 0.066, JNJ mean: 0.294 ± 0.041, p=0.012, U=25, Mann-Whitney U test), however the change in mean velocity (**b**) is not significant (p=0.060, U=3, Mann-Whitney U test), nor is the mean bout length during vehicle and JNJ (p=0.060, U=3, Mann-Whitney U test) (**d**) Comparison of mean number of bouts of each animal during vehicle and JNJ (p=0.403, U=8, Mann-Whitney U test). (**e**) Mean event rate of Ca^{2+} transients in dSPNs during movement. JNJ administration does not significantly affect the event rate in dSPNs (LMM, p=0.058, z=1.893, β=0.010, SE = 0.005, 95% CI: [-0.000 0.020], N=4 mice) (**f**) Coactivity of pairs of dSPNs (50 μm bins) during total time in open field. Systemic JNJ administration reduces pairwise coactivity (LMM, p=0.003, z=2.964, β=-0.450, SE = 0.152, 95% CI: [-0.153 0.748], N=4 mice) (**g**) Spatial coordination increases at movement onset in both vehicle and drug groups (VEH: p<0.000, z=6.249, JNJ: p<0.000, z=9.111, Wilcoxon Signed Rank test) (**i**) Normalized co-activity of dSPNs during rest. JNJ produces a small but significant reduction in coactivity measured during rest (velocity < 0.5 $cm*sec^{-1}$)(LMM, p=0.030, z=2.165, β=0.618, SE = 0.285, 95% CI : [0.059 1.177] , N=4 mice) (**j**) Normalized co-activity of dSPNs during movement (velocity > 0.5 $cm*sec^{-1}$). JNJ had a significant effect on dSPN clustered activity (LMM, p=0.027, z=-2.212, β=-1.694, SE = 0.766, 95% CI: [-3.195 -0.193], N=4 mice).(**k**) Event rate in dSPNs during vehicle and after JZL administration. JZL-184 administration reduces the event rate (LMM, p=0.001, z=3.195, β=0.007, SE = 0.002, 95% CI: [0.003 0.012] , N=5 mice) (**l**) Normalized co-activity of dSPNs against Euclidean distance. JZL had no effect on coactivity (LMM, p=0.065, z=-1.847, β=-1.204, SE = 0.652, 95% CI: [-2.481 0.074] , N=5 mice) (**m**) Time animals spent in velocity bins. JZL did not affect time spent at rest (p=0.531, U=16, Mann-Whitney U test).

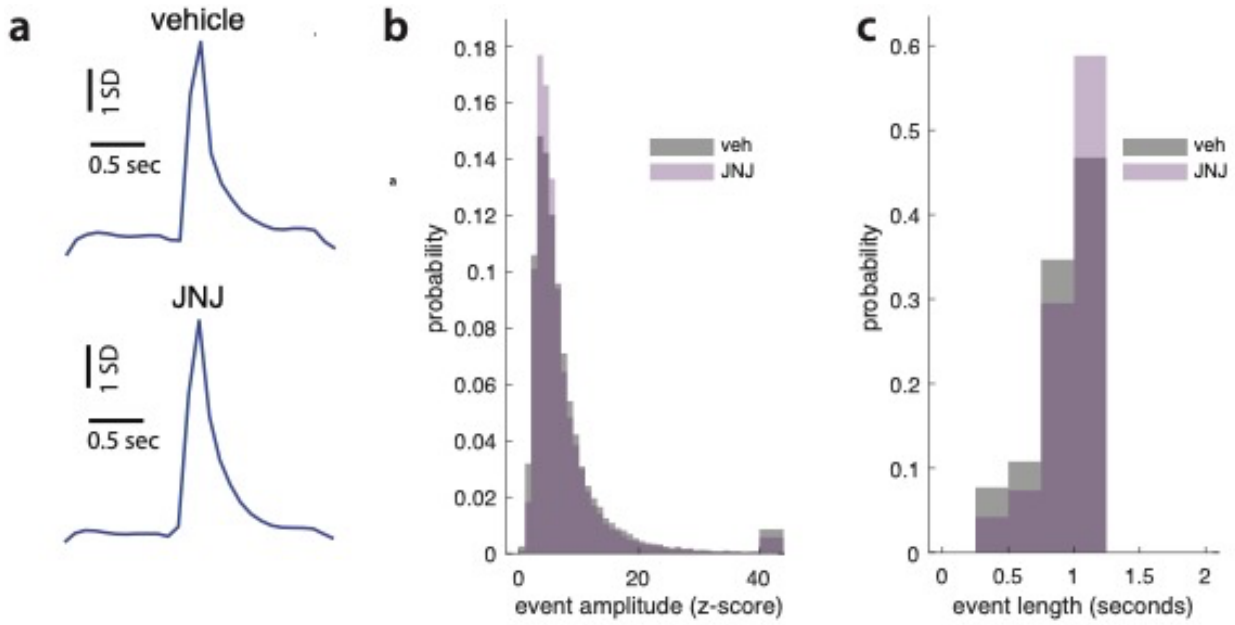

Figure 3 supplementary data

a) Averaged Ca^{2+} transients from vehicle and JNJ treated mice **b)** JNJ treatment does not affect the distribution of event amplitudes (LMM, p=0.955, z=0.056, β=0.048, SE=0.863, 95% CI: [-1.644 1.741], N=5 mice) **c**) JNJ treatment does not affect the distribution of event lengths (LMM, p=0.913, z=0.110, β=0.021, SE=0.188, 95% CI: [-0.348 0.389], N=5 mice)

1096 **Figure 3 – supplementary data 2**

1097

1098 Vehicle Sessions for JNJ experiments

Mouse	Total Cells	Sessions
2.20	111	2
2.21	150	2
2.25	671	3
2.24	107	2
2.26	199	2

1099

1100

1101 JNJ sessions

Mouse	Total Cells	Sessions
2.20	152	2
2.21	94	2
2.25	822	3
2.24	58	2
2.26	36	2

1102

1103 Vehicle Sessions for JZL experiments

Mouse	Total Cells	Sessions
2.8	150	4
2.14	129	2
2.19	203	2
2.20	80	2
2.26	22	2

1104

1105 JZL sessions

Mouse	Total Cells	Sessions
2.8	65	2
2.14	33	2
2.19	29	1
2.20	120	2
2.26	20	2

1106 **Table 3)** Number of cells per animal and recording sessions from animals used in figure

1107 3 analysis

1108

1109

1110

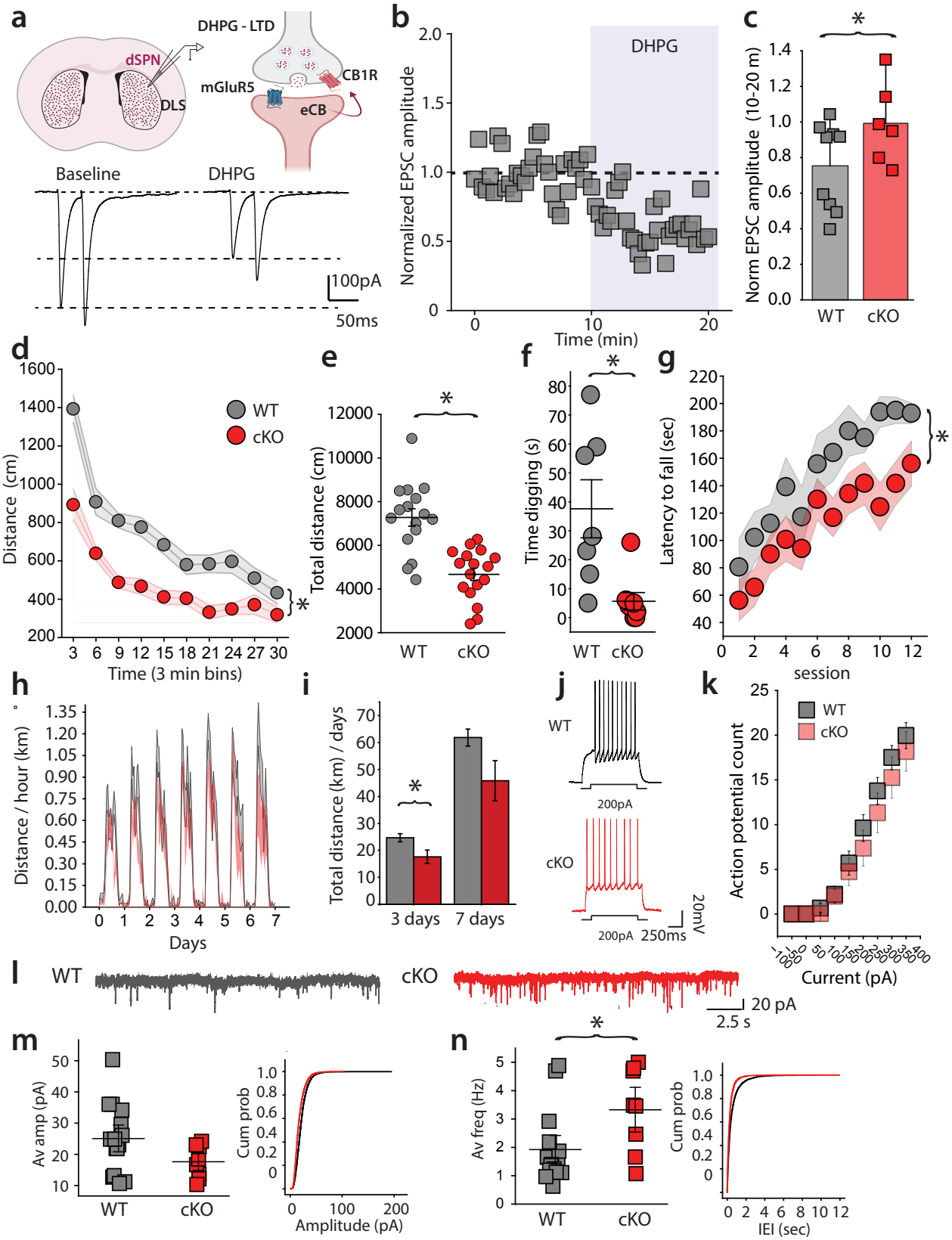
a
DHPG - LTD
dSPN
DLS
mGluR5
CB1R
eCB
Baseline
DHPG
100pA
50ms
b
DHPG
Normalized EPSC amplitude
Time (min)
c
Norm EPSC amplitude (10-20 m)
WT
cKO
d
Distance (cm)
Time (3 min bins)
WT
cKO
e
Total distance (cm)
WT
cKO
f
Time digging (s)
WT
cKO
g
Latency to fall (sec)
session
h
Distance / hour (km)
Days
i
Total distance (km) / days
3 days
7 days
j
WT
cKO
200pA
200pA
250ms
20mV
k
Action potential count
WT
cKO
Current (pA)
l
WT
cKO
20 pA
2.5 s
m
Av amp (pA)
WT
cKO
Cum prob
Amplitude (pA)
n
Av freq (Hz)
WT
cKO
Cum prob
IEI (sec)

1111

Figure 4) mGluR5 cKO in Drd1a-expressing neurons reduces spontaneous motor behaviors and affects synaptic properties of dSPNs

(**a**) (Top) Cartoon representation of the role of mGluR5 in mobilizing eCBs at corticostriatal synapses. (Bottom) Representative EPSCs recorded prior to and during DHPG in WT mice (**b**) Example time course of corticostriatal EPSCs recorded in dSPNs during application of 100 μM DHPG in slice from WT mice. (**c**) Grouped data of DHPG depression. D1 cKO mice lack DHPG induced synaptic depression (cKO normalized EPSC amplitude: 0.754 ± 0.082, Wilcoxon Signed Rank Test, p=0.018, W=2; WT normalized amplitude: 0.992 ± 0.992, Wilcoxon Signed Rank Test p=0.834, W=9). (**d**) Time course of activity in open field and (**e**) Total distance traveled by WT and cKO mice. D1 cKO mice have reduced activity in the open field, measured as distance traveled over time and total distance traveled during a 30-minute open-field session (Mann-Whitney U Test, U=245, p<0.001, N = 16 WT, 17 cKO). (**f**) Digging time in WT and cKO mice. D1 cKO mice spend less time digging when placed into a novel home cage (Mann-Whitney U Test, U=51.5, p=0.008, N = 7 WT, 8 cKO). (**g**) Latency to fall in the accelerating rotarod test. dSPN cKO mice have consistently reduced latency during the accelerating rotarod test over 3 days, with 4 sessions per day (p=0.024, F=5.709, Two-way repeated measures ANOVA, N = 12 WT, 17 cKO). (**h**) Running distance per hour on wireless wheels placed in home cage over 7 days. (**i**) Total distance run per day during first 3 days and over 7 days. D1 cKO mice ran significantly less during the first 3 days of testing (Mann-Whitney U Test, U=173, p=0.049) (**j**) Example traces of voltage response to 200pA current injection in WT and cKO mice. (**k**) There is not significant difference in the input output curve for current injection and AP firing between genotypes (LMM, p=0.056, z=1.913, β=1.197, SE = 0.626, 95% CI: [-0.029 2.424], N=26 cells, WT, N=22 cells, cKO). (**l**) Example mEPSC recordings in dSPN from WT and D1 cKO mice (**m**) Average amplitude of mEPSCs and cumulative distribution of amplitudes in WT and D1 cKO mice. There is no difference in amplitudes in recordings from the two genotypes (WT AMP: 21.04 ± 1.71 pA, N=15, cKO AMP: 16.66 ± 1.12, N=8, Mann-Whitney U Test, U=86.5, p=0.093) (**n**) Average mEPSC frequency and cumulative interevent intervals in WT and D1 cKO animals. D1 cKO mice have

1142 increased mEPSC frequency (WT Hz: 1.920 ± 0.3319 pA, N=15, cKO Hz: 3.325 ±
1143 0.525, N=8, Mann-Whitney U Test, U=27.5, p=0.039)

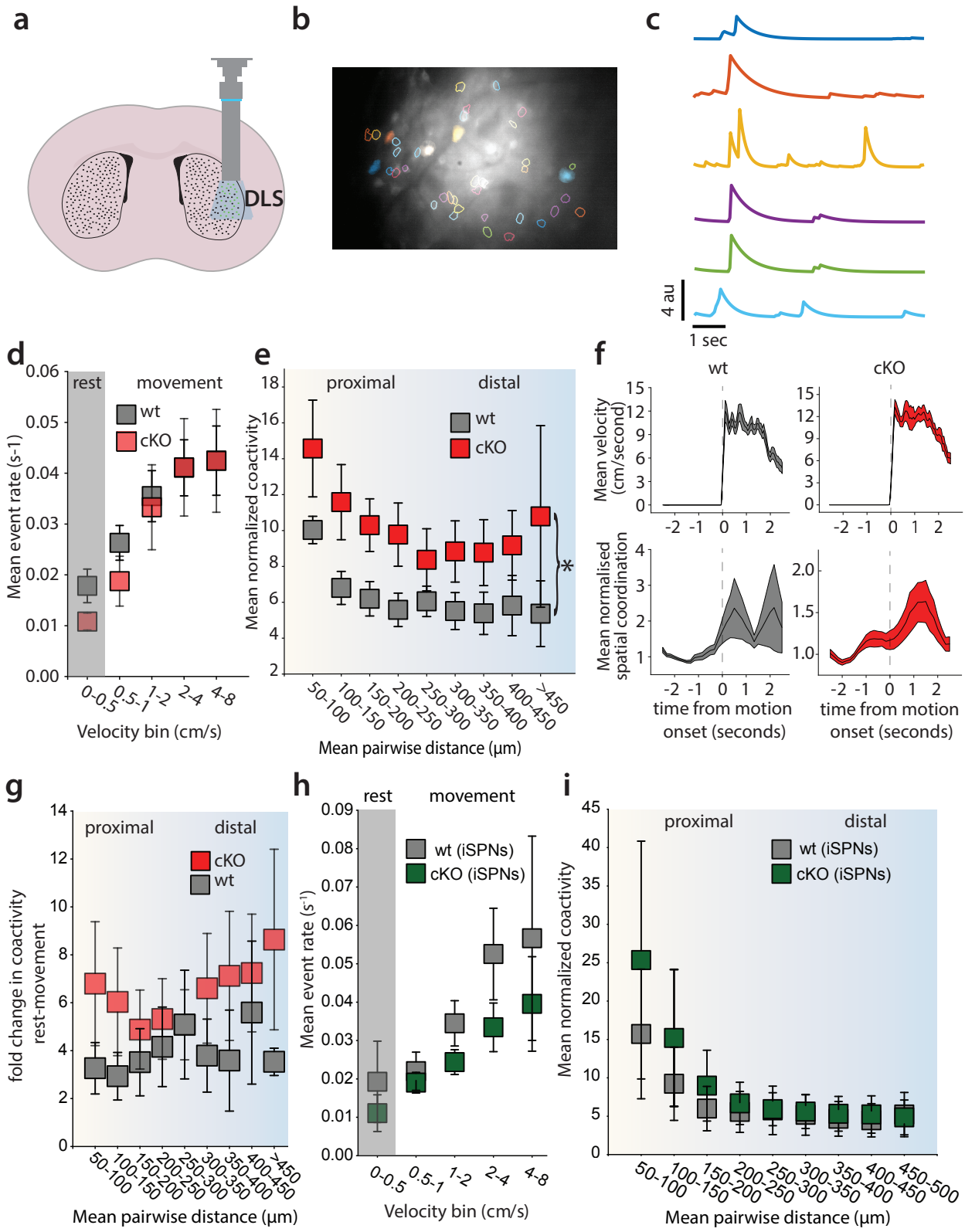
a
DLS
b
c
4 au
1 sec
d
rest
movement
wt
cKO
Mean event rate (s-1)
0-0.5
0.5-1
1-2
2-4
4-8
Velocity bin (cm/s)
e
proximal
distal
wt
cKO
Mean normalized coactivity
50-100
100-150
150-200
200-250
250-300
300-350
350-400
>450
Mean pairwise distance (µm)
f
wt
cKO
Mean velocity (cm/second)
Mean normalised spatial coordination
time from motion onset (seconds)
g
proximal
distal
cKO
wt
fold change in coactivity rest-movement
Mean pairwise distance (µm)
h
rest
movement
wt (iSPNs)
cKO (iSPNs)
Mean event rate (s-1)
Velocity bin (cm/s)
i
proximal
distal
wt (iSPNs)
cKO (iSPNs)
Mean normalized coactivity
450-500
Mean pairwise distance (µm)

1144

Figure 5) D1 cKO mice show cell autonomous increase in clustered coactivity in dSPNs

(**a**) Cartoon representation of miniscope imaging in the DLS (**b**) Example segmented image from cKO mice (**c**) Example Ca^{2+} activity traces from identified dSPNs in cKO mice, filled cells in (b) (**d**) Mean event rate during movement in WT and cKO animals. The event rate in dSPN cKO mice is unchanged from WT (LMM, p=0.651, z=0.452, β=0.003, SE = 0.007, 95% CI: [-0.011 0.017] , N=9 wt, 6 cKO) (**e**) Coactivity of pairs of dSPNs (50 μm bins) in WT and cKO animals. D1 cKO mice have increased coactivity across all pairwise distances (MLM, p=0.021, z=2.305, β=3.989, SE = 1.731, 95% CI : [0.597 7.382] , N=9 wt, 6 cKO) (**f**) Spatial coordination peaks at movement onset in both wt and cko mice (WT: p<0.000, z = 7.301, KO: p<0.000, z = 6.700, Wilcoxon Signed Rank test) (**g**) The relative increase in coactivity during rest is not statistically different between cKO and wt mice (LMM, p=0.552, z=0.595, β=1.391, SE=2.339, 95% CI: [-3.193 5.976]) (**h**) iSPN event rate in D1 cKO and WT animals is unchanged (LMM, p=0.310, z=1.016, β=0.017, SE = 0.016, 95% CI: [-0.015 0.048], N=3 wt, 3 cKO) (**i**) Clustered coactivity of iSPNs in WT and D1 mGluR5 cKO animals is unaffected (LMM, p=0.691, z=0.398, β=2.368, SE = 5.953, 95% CI: [-9.300 14.035], N=3 wt, 3 cKO).

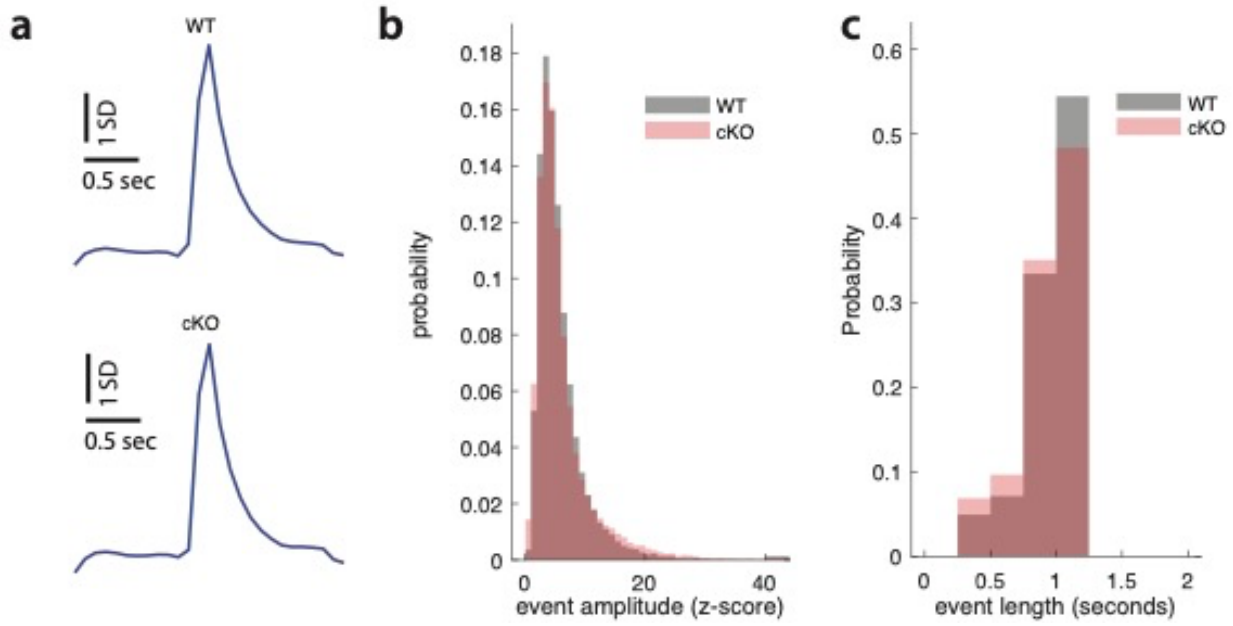

Figure 5 supplementary data 1

a) Averaged Ca^{2+} transients from wt and cKO mice **b)** Wt and cKO mice show similar distributions of event amplitudes (LMM, p=0.497, z=-0.679, β=-0.177, SE=0.261, 95% CI: [-0.690 0.335], N=5 mice) **c**) Wt and cKO mice show similar distributions of event length (LMM, p=0.284, z=1.072, β=0.140, SE=0.130, 95% CI: [-0.116 0.395], N=5 mice)

1185 **Figure 5 supplementary data 2**

1186 WT (D1 cre ; *GRM5* +/+) – dSPNs

Mouse	Cells	Sessions
2.1	23	1
2.19	83	2
1.13	35	1
1.26	22	2
1.27	45	1
1.32	237	2
1.33	128	2
1.35	280	3
1.39	159	3

1187

1188 cKO (D1 cre ; *GRM5* f/f) - dSPNs

Mouse	Cells	Sessions
1.9	143	1
1.11	202	1
1.12	139	2
1.18	104	2
1.38	377	3
1.41	2	1

1189

1190 WT (D1 cre ; *GRM5* +/+) – iSPNs

1191

Mouse	Cells	Sessions
DO_1	114	1
DO_2	125	1
DO_3	39	1

1192

1193 cKO (D1 cre ; *GRM5* f/f) – iSPNs

1194

Mouse	Cells	Sessions
DO_4	63	1
DO_5	116	1
DO_6	221	1

1195

1196 **Table 5)** Number of cells per animal and recording sessions from animals in figure 5

1197

1198